Draft version January 4, 2022
Typeset using LaTeX **twocolumn** style in AASTeX631

Transit Hunt for Young and Maturing Exoplanets (THYME) VIII: a Pleiades-age association harboring a transiting planet from *Kepler* (NOW TWO TRANSITING SYSTEMS)

Madyson G. Barber,[1] Andrew W. Mann,[1] Benjamin M. Tofflemire,[2,*] Jonathan L. Bush,[1] Adam L. Kraus,[2] Daniel Krolikowski,[2] Andrew Vanderburg,[3] Matthew J. Fields,[1] Elisabeth R. Newton,[4] Dylan A. Owens,[1] and Mackenna L. Wood[1]

[1] *Department of Physics and Astronomy, The University of North Carolina at Chapel Hill, Chapel Hill, NC 27599, USA*
[2] *Department of Astronomy, The University of Texas at Austin, Austin, TX 78712, USA*
[3] *Department of Physics and Kavli Institute for Astrophysics and Space Research, Massachusetts Institute of Technology, Cambridge, MA 02139, USA*
[4] *Department of Physics and Astronomy, Dartmouth College, Hanover, NH 03755, USA*

ABSTRACT

We describe a young association (MELANGE-2) in the *Kepler* field with a known planet candidate (KOI-3876.01) with signs of youth. To better determine the age and membership of MELANGE-2, we combine archival light curves, velocities, astrometry, with new high-resolution spectra of stars nearby KOI-3876.01 spatially and kinematically. The resulting rotation sequence, lithium levels, and color-magnitude diagram of members are all an excellent match for the Pleiades, confirming the population is co-eval and providing an age estimate of 110±10 Myr. KOI-3876's observed properties are an excellent match to the group, confirming membership. MELANGE-2 may be part of the larger Theia 316 stream, also estimated to be ≃108 Myr. For KOI-3876, we revise the stellar and planetary parameters of the system, taking into account the newly-determined age. We fit the 4.5 yr light curve from *Kepler* and find that KOI-3876.01 is a $2.0 \pm 0.1 R_\oplus$ planet that orbits its star every 19.58 days on an eccentric ($e > 0.2$) orbit. KOI-3876 was previously flagged as a likely eclipsing binary, but we rule this out using radial velocities from APOGEE and statistically validate the signal as planetary in origin based on archival follow-up and its *Kepler* light curve. Given its overlap with the *Kepler* field, we expect MELANGE-2 to be valuable for studies of spot evolution on timescales of years and KOI-3876 to be a piece of the growing work on transiting planets in young stellar associations.

Keywords: exoplanets, exoplanet evolution, young star clusters- moving clusters, planets and satellites: individual (KOI3876)

1. INTRODUCTION

Stellar clusters and associations serve as critical benchmarks for stellar and planetary astrophysics. Stars in such groups formed from the same interstellar cloud, and hence share a common (or similar) age, abundance pattern, and initial space velocity. The common set of properties makes it significantly easier to assign properties to the whole population, providing age estimates that are more precise and accurate than general-purpose techniques used outside clusters (e.g., Gyrochronology; Barnes 2007; van Saders et al. 2016) and work on stars where ages are especially challenging (e.g., M dwarfs; Kiman et al. 2021). Such coeval associations are therefore, ideal for how studying how stellar and planetary properties evolve with time (Krumholz et al. 2019; Mann et al. 2016a).

Associations within the *Kepler* field have been especially valuable for stellar and planetary astrophysics. The ≃4.5 yr baseline and precise photometry enable precise measurements of rotation periods, even at older ages (e.g., Angus et al. 2015; Aigrain et al. 2015), providing some of the best constraints we have on the rotation evolution of stars past 1 Gyr (Meibom et al. 2011; Curtis et al. 2019). The four *Kepler* clusters (NGC 6866, NGC 6811, NGC 6819, and NGC 6791) have also provided

Corresponding author: Madyson G. Barber
madysonb@live.unc.edu

* 51 Pegasi b Fellow

a wealth of information about stellar mass-loss (Miglio et al. 2012), post-main-sequence stellar evolution (Corsaro et al. 2012), and the occurrence of planets inside clusters (Meibom et al. 2013).

The four known clusters in the *Kepler* field are all at distances of more than 1 kpc and ages $\gtrsim$500 Myr. While these older ages (compared to nearby young groups) fill an important niche in stellar spin down and post-main-sequence evolution, their distance from the Sun makes it challenging to study the low-mass members and search for small planets. The *K*2 mission covered many younger and more nearby clusters (Van Cleve et al. 2016; Rizzuto et al. 2017), but only for $\simeq$80 days at a time. Searching for long-period planets and studying longer-term spot evolution with *K*2 data was therefore only possible in regions that *K*2 covered by multiple campaigns (Rampalli et al. 2021). Additional young associations in the *Kepler* field would provide the invaluable $\simeq$4.5 yr baseline.

The availability of precise parallaxes and proper motions for millions of stars from *G*aia (Gaia Collaboration et al. 2016, 2021) has enabled the discovery of new coeval stellar associations (e.g., Meingast et al. 2019; Kerr et al. 2021). The `FriendFinder` code[1] (Tofflemire et al. 2021) was designed to take advantage of *G*aia data, by searching for potential co-moving 'friends' around a user-identified young stars. This method has already been useful in finding the 250 Myr MELANGE-1 association (Tofflemire et al. 2021) and age-dating a planet in the Musca region of Lower-Centarus-Crux (Mann et al. 2021).

With the goal of finding previously undiscovered associations with transiting planets, we ran `FriendFinder` on *Kepler* objects of interest suspected to be younger than Hyades based on their lithium levels in Berger et al. (2018). The most promising association was a group of stars nearby KOI-3876; the candidate members showed a color-magnitude diagram (CMD) consistent with the Pleiades (consistent with the lithium levels). Here we describe our work demonstrating that the population (MELANGE-2) is a co-eval 110 Myr group, $\simeq$300 pc from the Sun, and harbors two transiting planetary systems (KOI-3876 b and Kepler-970 b).

While the THYME survey was meant to focus on planets identified with *TESS*, KOI-3876 b was flagged as young by the same team and using the same methods as used extensively in the THYME and ZEIT series. Since the planet is not along the ecliptic, we opted to include it in the THYME survey series with a slight adjustment to the acronym.

The paper is organized as follows. In Section 2 we detail our initial selection of potential members of MELANGE-2. We list the range of archival and new data taken on candidate members of MELANGE-2 in Section 3. In Section 4 we demonstrate MELANGE-2 is a co-eval population and derive its overall properties and basic membership. Our effort to find known and new planets in MELANGE-2 is described in Section 5. We derive properties of the only identified planet in the association, KOI-3876 b, in Section 7, and statistically validate it in Section 7.1. We summarize our findings in Section 8 and briefly discuss the future utility of an association overlapping the *Kepler* field.

2. TARGET SELECTION

As part of our effort to identify known planets in previously undiscovered young associations we ran the `FriendFinder` code (Tofflemire et al. 2021) on all stars identified as young based on their lithium absorption (Berger et al. 2018); this initial seed list included KOI-3876. The `FriendFinder` algorithm uses *G*aia EDR3 positions, parallaxes, and proper motions to identify stars with similar Galactic tangential velocity and XYZ position to a selected input source. This required an absolute velocity for KOI-3876, for which we used the value from APOGEE (-26.79km s^{-1}, Jönsson et al. 2020).

The lithium levels suggested an age for KOI-3876 close to the Pleiades. Unbound or weakly bound associations >100 Myr should be significantly dispersed as they orbit through the Galaxy (this needs a citation). So we used a generous selection, including any star within 5km s^{-1} and 50 pc of KOI-3876 as a candidate member. This yielded 1007 candidates.

We show the color-magnitude diagram (CMD) for our candidate members in Figure 1. The spread of the CMD suggests significant contamination; it is likely that most of the 1007 stars selected are not associated with KOI-3876. However, the CMD also shows there is significant contamination, there is also a sequence of the closest stars (in tangential velocity) consistent with the Pleiades single-star sequence. This matches the age suggested by the Li levels in KOI-3876.

3. OBSERVATIONS

3.1. *Optical spectra from McDonald 2.7 m Coudé*

We observed KOI-3876 and 21 association candidates (Section 2) with the Coudé spectrograph on the Harlan J. Smith 2.7m telescope at the McDonald Observatory. The Robert G. Tull Coudé is a cross-dispersed echelle spectrograph, delivering a R$\sim$60,000 spectral resolution

[1] https://github.com/adamkraus/Comove

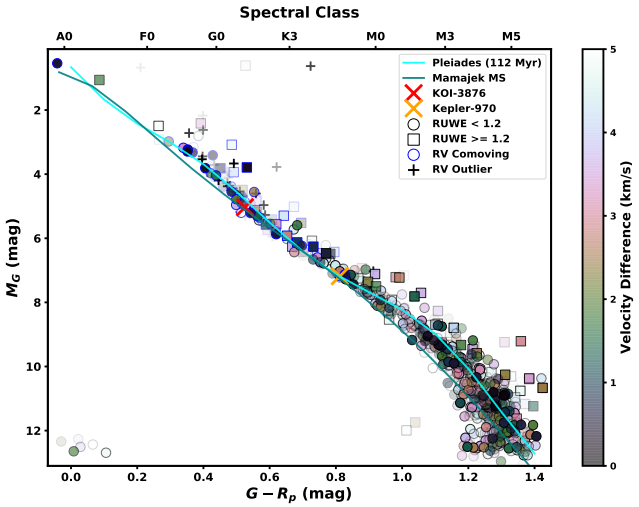

Figure 1. *G*aia color-magnitude diagram of all stars within 5 km s^{-1} in tangential velocity 50 pc (right) of KOI-3876. Approximate spectral types are shown on the top axis. Points are color-coded by the difference between their expected and observed tangential velocity assuming a perfect *UVW* match to KOI-3876 and transparency based on their distance from KOI-3876. Points with radial velocities consistent with KOI-3876 are marked with blue circles and those with discrepant velocities are changed to a plus signs (and excluded from the color coding). Approximate main Pleiades single-star sequences are shown as colored lines. These sequences are not corrected for reddening, and are only used as a rough guide.

from 3400–10000 Å using the 1.″2 slit (Tull et al. 1995). Observations we're taken over the course of two observing runs, on 2021 July 9 and 2021 August 26–27. The sample was selected to include association candidates that could be observed with the Coudé in modest exposure times ($G < 13$), and spectral types later than mid-F ($B_p - R_P > 0.55$), where we expect lithium absorption to be a sensitive age diagnostic. The spectra are reduced with a custom python implementation of the standard IRAF procedures. Wavelength calibration made use of ThAr lamp spectra taken at the beginning, middle, and end of each night. the signal-to-noise of our spectra ranged between 14 and 60 per resolution element.

To assess whether association candidates are comoving in three dimensions, we measure radial velocities using spectral-line broadening functions (BFs). The BF is a linear inversion of an observed spectrum with a narrow-lined template, and represents the average stellar absorption-line profile. This profile (the BF) can be fit with a rotationally-broadened line profile to measure the stellar radial velocity and $v \sin i_*$. We compute BFs for 34 spectral orders between 4300 and 9800 Åthat are free of telluric contamination using the `saphires` python package (Tofflemire et al. 2019). BFs from individual orders are combined in to a single, high SNR BF and fit with a rotationally broadened profile (Gray 1992). Narrow-lined templates, specific to each star, are taken from the Husser et al. (2013) PHOENIX model suite at the $T_{\rm eff}$ closest to that provided by the *TESS* Input Catalog (v8.0; Stassun et al. 2019). Radial-velocity errors depend on the S/N and rotational broadening, but are generally on the order of 0.1 km s^{-1}. Measurements from the Coudé spectra are provided in Table 5.

3.2. *Kepler and TESS light curves*

3.2.1. *Light curves for transit search and characterization*

We searched for *Kepler* photometry for all 1007 candidates within the Mikulski Archive for Space Telescopes (MAST). A total of 84 targets had *Kepler* data, the majority of which had data from all quarters (Q0-Q17). We restricted our analysis to long-cadence data (30 m), as short-cadence was not available for any of the candidate planet hosts and short cadence data is not needed for our transit search or rotation estimates. For those lacking *Kepler* data, we instead downloaded *TESS* photometry wherever it was available through MAST. This included 15 targets with 2-minute cadence data, and 41 targets with 30-minute cadence data from the Quick-Look Pipeline (QLP; Huang et al. 2020).

Where possible, we used the Pre-search Data Conditioning Simple Aperture Photometry (PDCSAP; Smith et al. 2012; Stumpe et al. 2012). This included KOI-3876, all *Kepler* candidate members, and the 15 targets with 2-minute cadence from *TESS*. For the remaining, we used the Quick-Look Pipeline light curves (Huang et al, 2020; https://arxiv.org/abs/2011.06459) for our planet search. Table 5 lists which stars have *Kepler* and/or *TESS* photometry that was used for our planet search. More details on our transit search can be found in Section 5.

The remaining 885 sources had no pre-extracted *TESS* or *Kepler* light curves. We did not extract additional curves from the full-frame *TESS* images for our planet search or characterization. The association is more than 300 pc away; most of the remaining stars were too faint to extract a light curve precise enough for our planet search. However, many such systems are still useful for measuring rotation periods.

3.2.2. *Light curves and literature search for rotation*

To assess membership and age of MELANGE-2 members, we collect stellar rotation periods using literature measurements supplemented by our own measurements from *Kepler* and *TESS* light curves. First, candidate members were cross matched against Nielsen et al.

(2013), McQuillan et al. (2013, 2014), and Santos et al. (2019, 2021) for literature rotation periods. We matched candidate members to catalog members by *Kepler* Input Catalog (KIC) identifiers, which are listed in each catalog. We identified 56 candidate members with available literature rotations, all but five of which have rotation measurements in multiple catalogs. For candidates that appear in only one catalog, we adopt the single measurement value. In cases where a star had measurements from more than one source, we adopt the average of the measurements as the rotation period. Only one object, KIC 3743810, had a conflicting rotation periods between catalog sources. Based on a visual examination of this object's *Kepler* PDCSAP light curve we selected the value from Nielsen et al. (2013).

For stars without literature rotation periods we performed our own analysis. Priority was given to *Kepler* PDCSAP data followed by *TESS* full-frame images. To generate the *TESS* light curves for rotation analysis, we first created raw flux light curves from the FFI cutouts centered on each candidate. Then, we generated a Causal Pixel Model (CPM) of the telescope systematics using the `unpopular` package (Hattori et al. 2021) for each individual star. We subtracted the CPM systematics from the initial light curves, resulting in the light curves used for our rotation search described in Section 4.2.

3.3. *Archival photometry and astrometry*

We download positions, parallaxes, proper motions, and B_P, R_P and G photometry for all candidate members of MELANGE-2 using the third *G*aia Early Data Release (EDR3; Gaia Collaboration et al. 2021). For KOI-3876, we also retrieved photometry from the Two-Micron All-Sky Survey (2MASS; Skrutskie et al. 2006), the Wide-field Infrared Survey Explorer (WISE; Cutri & et al. 2014), and the AAVSO All-Sky Photometric Survey (APASS; Henden et al. 2016). Photometry for KOI-3876 is listed in Table 3.

3.4. *Archival Velocities*

In order of preference, we drew radial velocities for candidate MELANGE-2 members from the second *G*aia data release (DR2; Katz et al. 2019), the sixteenth APOGEE data release (DR16; Jönsson et al. 2020), and the fifth LAMOST data release (DR5; Luo et al. 2015, 2019). Velocities from our own spectra (Section 3.1) were given the highest priority. In the instance where a star had multiple velocities from the same star we used the weighted mean and error. We did not combine multiple velocities from different sources due to possible differences in the zero-points.

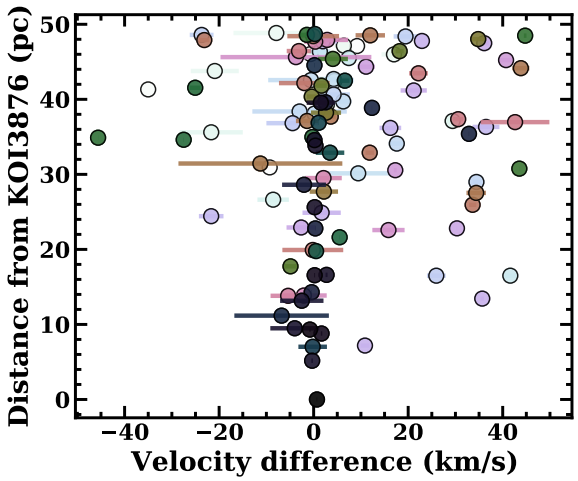

Figure 2. Radial velocities of candidate members of MELANGE-2.

In total, we adopted *G*aia RVs for 56 stars, APOGEE RVs for 5 stars, and LAMOST RVs for 25 stars. This was in addition to velocities from our Coude spectra for 22 candidate member stars as well as KOI-3876. We applied an offset to the LAMOST velocities of +4.54km s^{-1} based on the comparison from Anguiano et al. (2018). There may be additional zero-point differences between the velocity sources, but these are likely larger than the internal velocity spread within the group. The adopted velocities are given in Table 5.

4. THE MELANGE-2 ASSOCIATION

As we show in Figure 2, radial velocities of candidate members are heavily clustered near the values we expect if their Galactic UVW velocities match KOI-3876 within a couple km s^{-1}. The over-density is also highest for stars closer to KOI-3876 in tangential velocity and position.

Since the initial selection of targets was done without radial velocity information (Section 2) the abundance of similar radial velocities cannot be due to chance. Given the radial velocity of a expected typical thin disk star with similar XYZ to KOI-3876 (Bochanski et al. 2007; **?**), the probability of such a buildup is negligibly small. This demonstrates that the association is a real group. We denote this group as MELANGE-2 (Membership and Evolution by Leveraging Adjacent Neighbors in a Genuine Ensemble), following the naming convention in (Tofflemire et al. 2021).

The distribution in Figure 2 also highlights a problem; there is a significant population of stars with velocities far outside expectations for membership. Such contaminants include stars near KOI-3876 in position and kine-

matics. Further, the overdensity in velocity space is not necessarily co-eval; overdensities in kinematic space can occur for other reasons, such as dynamical perturbations from the Galactic bar (**?**).

Our goal for the rest of this section is to demonstrate that MELANGE-2 is a single-age population and determine its age and basic kinematic and position properties.

4.1. *Lithium*

We measured the equivalent width of the Li 6708 Å line for 22 stars (including KOI-3876) using the Coude spectra described in Section 3.1. Using our measured radial and rotation velocities from the BF analysis, we shifted each spectrum to zero velocity and compared it to a rotationally broadened template of the same $T_{\rm eff}$. We then interactively defined regions of continuum between 6685 and 6730 Å, and the bounds of the EW integration. We measured the Li EW and its uncertainty using a bootstrap approach. The continuum was first fit using `emcee`, 1000 random draws from the fit posterior are used to normalized the spectrum, and for each realization, the Li absorption line is numerically integration 10 times where the integration bounds are varied randomly from a normal distribution with the width of a resolution element. This procedure results in 10,000 Li EW measurements, we take the median and standard deviation as our final measurement and its uncertainty, respectively.

Past detections of Li with the same observational setup and our typical spectrum SNR indicate we were sensitive to Li down to equivalent widths of $20 m\mathring{A}$ or better. So we report this as our upper limit when no line is detected. One star (Gaia EDR3 2052858307226740352) had a $v \sin i_* >$ 50km s^{-1}, which made extraction of the Li line unreliable. So we instead reported a $< 70 m\mathring{A}$ upper limit for this source based on earlier detections on similarly broadened spectra.

For KOI-3876, we estimated a Li equivalent width if 134 $m\mathring{A}$. This is marginally higher than (but consistent with) the value from Berger et al. (2018) (120 $m\mathring{A}$). We attribute this difference to Berger et al. (2018)'s removal of the Fe line at 6707.44 Å. We did not attempt to correct for this contamination or from broad molecular contamination in the cooler stars. Fe line contamination likely set a limit on the precision of our equivalent widths at the $\simeq$10% level, comparable to the measurement errors. The difference was small compared to the offset in Li levels between clusters; we used our Li measurements for all targets for consistency.

Two spectra (Gaia EDR3 2101333021814076800 and 2048317736525727488) had two clear sets of lines, indicating an SB2. For our Li measurements, we measured each line individually with a manually-applied velocity offset. We then combined the two equivalent widths.

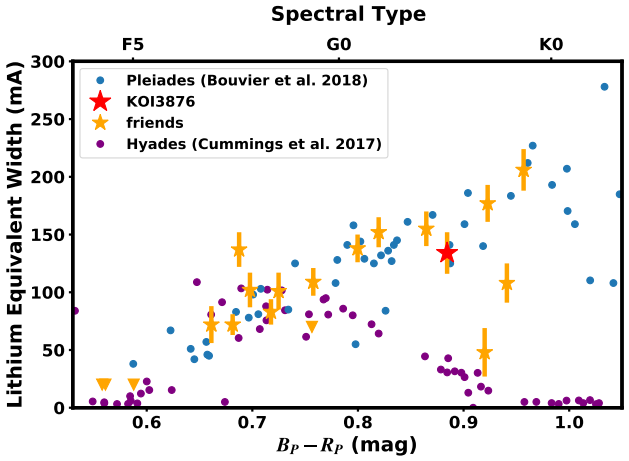

Figure 3. Lithium equivalent width as a function of *Gaia* $B_P - R_P$ color for candidate members of KOI-3876 (MELANGE-2; orange), KOI-3876 (red), and members of the 125 Myr Pleiades from Bouvier et al. (2018) and $\simeq$700 Myr Hyades (Cummings et al. 2017). Triangles indicate upper limits. We have excluded MELANGE-2 candidates with velocities inconsistent with membership. The MELANGE-2 sequence is consistent with that from Pleiades members; only one star has an anomalously low Li (Gaia EDR3 2044150037698600448) compared to the Pleiades sequence. The high levels of Lithium seen in the mid-G dwarfs alone demonstrate that MELANGE-2 is much younger than Hyades.

We compared the Li sequence for MELANGE-2 to that from the $\simeq$112 Myr Pleiades Bouvier et al. (2018) and the 650-700 Myr Hyades from (Cummings et al. 2017) in Figure 3. The MELANGE-2 sequence is nearly identical to that from Pleiades. The Li sequences of nearby clusters from `BAFFLES` (Stanford-Moore et al. 2020) suggested an age between 85 Myr and 200 Myr This age range is conservative, as the bounds can only be set using the set of clusters with ages and extant lithium sequence measurements. For the upper bound, this was set by M34 and M35 (200-300 Myr).

4.2. *Rotation*

To better constrain the age and membership of MELANGE-2 (and hence KOI-3876), we attempted to determine rotation periods for all candidate members using *Kepler* rotation measurements from the literature or our own measurements from *Kepler* data or *TESS* full-frame images (FFIs). The light curve extraction and literature search are described in Section 3.2.2.

For our own measurements, we searched the single-quarter *Kepler* or *TESS* light curves for rotation periods between 0.1 – 50 days using the Lomb-Scargle al-

gorithm (Horne & Baliunas 1986) for each quarter for each star with available *Kepler* data. We selected the initial rotation from the quarter returning the rotation period with the highest periodogram power. To confirm these measurements, we phase-folded the single-quarter light curves to the discovered period and examined the signals' consistency across quarters. We performed an eye-check in the style of Rampalli et al. (2021), labeling obvious rotations as Q0, questionable rotations as Q1, spurious detections as Q2, and non-detections as Q3. In total, 11 of the stars with *Kepler* data and no literature rotation returned usable rotations of quality Q0 or Q1.

For the rest of the candidates without rotations found in the literature or through our *Kepler* light curve measurements, we searched for signatures of rotation in CPM light curves extracted from the *TESS* Full Frame Image data (see Section 3.2). After searching each single-sector light curve of each star for rotation periods from 0.1−30 days using the Lomb-Scargle algorithm, we repeated the same rotation selection and quality check procedure as outlined for the *Kepler* data. We found 64 quality Q0 or Q1 rotations from the *TESS* CPM-subtracted light curves available.

Based on variations in the extracted rotation period between *TESS* sectors and/or *Kepler* quarters, we estimate rotation period errors to be ≃10% for our own measurements. This larger than the expected errors just considering signal-to-noise and Lomb-Scargle errors from bootstrapping, likely due to differential rotation and spots appearing and disappearing on the surface of the star.

In total, we were able to assign rotation periods to 131 candidate members, all of which are reported in Table 5; 67 periods were determined based on *Kepler* data and 64 from *TESS*. The rotation period distribution (Figure 4) is extremely consistent with that from the Pleiades, further validating the age from our Li measurements and isochrone fit. Approximately 92 of these have rotation periods consistent with the Pleiades sequence. Most of the slower rotators are likely field interlopers, as they are (statistically) further from KOI-3876 in both three-dimensional distance and tangential velocity.

Of 1007 initial candidates, only having 92 stars with Pleiades-like rotation periods initially appears as a low success rate for a young association. However, the overwhelming majority of the other 876 stars were stars where no rotation period could be measured even if one is present (mostly due to intrinsic faintness). For example, of the 935 stars with a matching TIC ID, but no rotation period from *Kepler* data, 751 were either too faint ($T \gtrsim 15$) or too contaminated by nearby stars to extract a usable CPM curve. An unknown further set

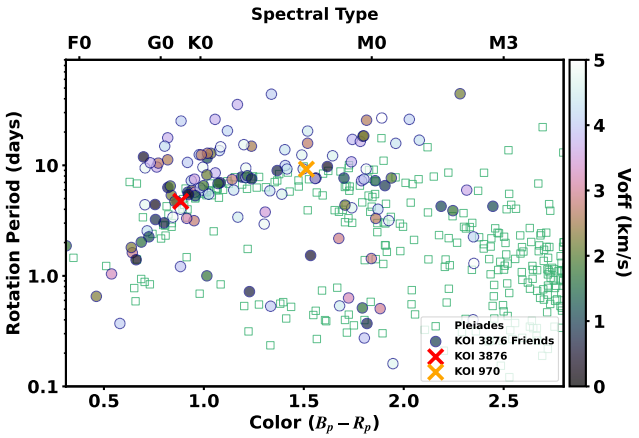

Figure 4. Rotation periods candidate members of MELANGE-2 (dark circles). Only literature measurements or stars with Q0 or Q1 rotations are shown. For reference, we show rotation periods from ≃110 Myr Pleiades (green squares; cite Rebull 2016 Multiperiod Pleiades stars). Stars are color-coded by their tangential velocity difference compared to KOI-3876. Statistically, the stars on the Pleiades gyrochrone are also closer to KOI-3876 in tangential velocity. Because of the distance to the cluster, we have few rotation periods past M1.

of stars had light curves but may have had rotation amplitudes below detectable levels due to poor SNR. Thus, the difference is mostly a measure of how *G*aia can retrieve precise astrometry for stars far fainter than *Kepler* and *TESS* can provide rotation periods for.

4.3. *Galactic Position and Kinematics*

For each of the 1007 candidate members of MELANGE-2, we show show the Galactic XYZ position in Figure 6 and the proper motion in Galactic coordinates (l, b) in Figure 5. While there is a clear overdensity of sources within ≃1km s^{-1} of KOI-3876 and Kepler-970, four initial selection included a large number of field contamants. A tighter cut on velocity and distance would lower contamination, but some sources far in separation have matching velocities and show other signs of youth (such as rotation). This makes it challenging to derive the $UVWXYZ$ parameters of the association from the full membership list.

Instead, we select a set of high probability members independent of their *G*aia parameters that were used for initial selection. We included only sources with a rotation period consistent with the Pleiades sequence and those with radial velocities within 10km s^{-1} of the source. We removed three additional targets that had low-precision velocities (from LAMOST).

The cuts left us with 31 high-probability members. From these we estimate the Galactic position (XYZ) and kinematic (UVW) parameters, as well as the clus-

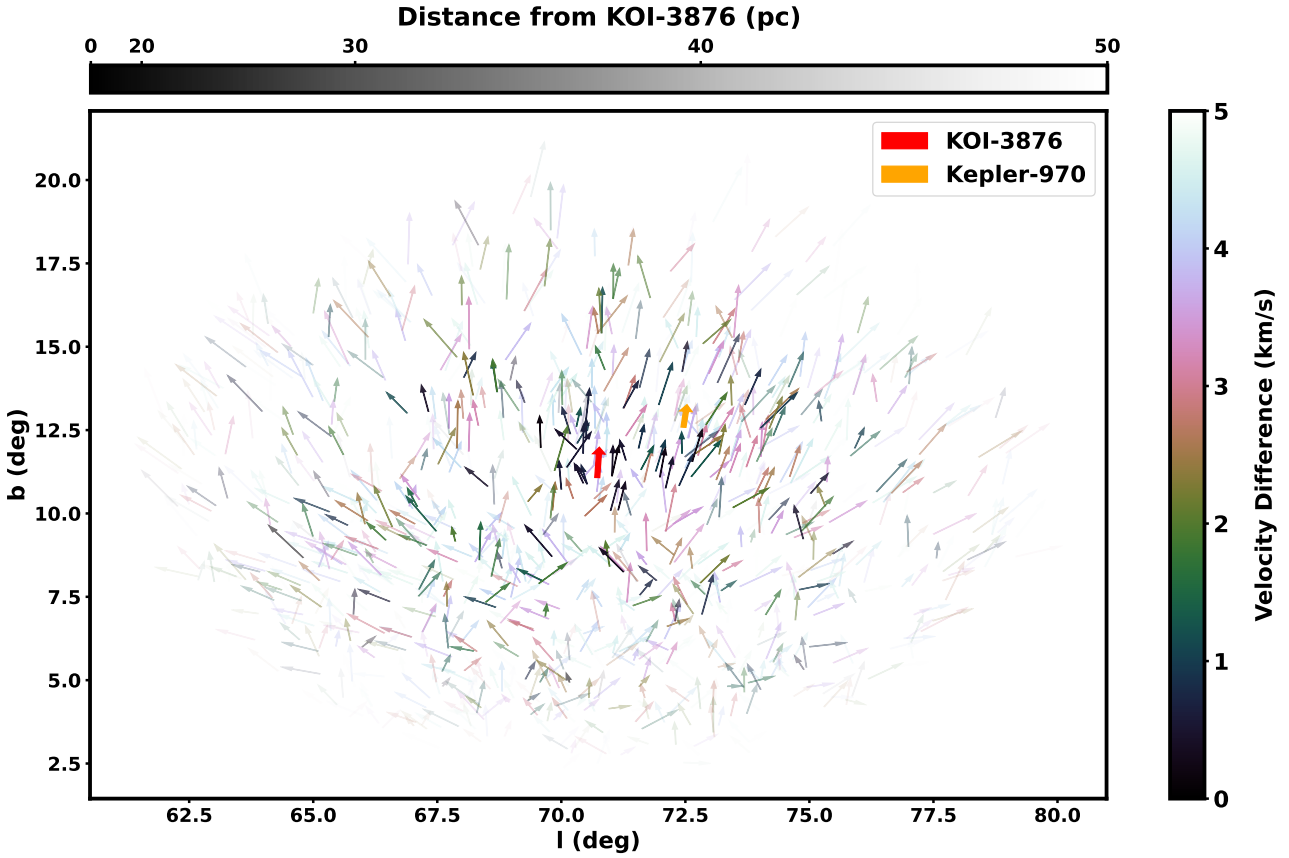

Figure 5. Galactic coordinates and motions for all 1007 candidate members of MELANGE-2. The red arrow shows KOI-3876, Kepler-970 is shown in orange, and other stars are color-coded by their tangential velocity offset from KOI-3876 with transparency set by their physical distance from KOI-3876. Arrows indicate the direction and (relative) magnitude of the proper motion.

Table 1. Properties of MELANGE-2

Parameter	KOI-3876	Kepler-970	Source
	Name		
X (pc)	103	19	
Y (pc)	289	18	
Z (pc)	63	14	
U (km s^{-1})	-9.2	1.4	
V (km s^{-1})	-25.54	0.36	
W (km s^{-1})	1.0	1.2	

ters in each parameter (σ_X, σ_Y, σ_Z, σ_U, σ_V, and σ_W) after accounting for measurement errors. The resulting parameters are given in Table 1.

A more formal treatment would account for covariance between these parameters (e.g., Gagné et al. 2018). However, the group may actually be part of a much larger stellar stream, which would require a different model (Kounkel & Covey 2019; Gagné et al. 2021). We discuss this possibility in more detail in Section 8.1. Since we were primarily interested in characterizing the planets, we defer a more detailed analysis of MELANGE-2 and its relation to other groups for a pure association analysis.

4.4. *Isochronal age*

We estimated the age of MELANGE-2 by comparing the CMD to the PARSEC (v1.2S) models (Bressan et al. 2012). We used a mixture model, as detailed in Mann et al. (2021)[2], based on the method outlined in Hogg et al. (2010), and wrapped in a Monte-Carlo Markov-Chain using `emcee` (Foreman-Mackey et al. 2013). To briefly summarize, we fit the population with the combination of two models. The first described the single-star member sequence drawn from PARSEC models. The second is an outlier population, which may itself contain

[2] https://github.com/awmann/mixtureages

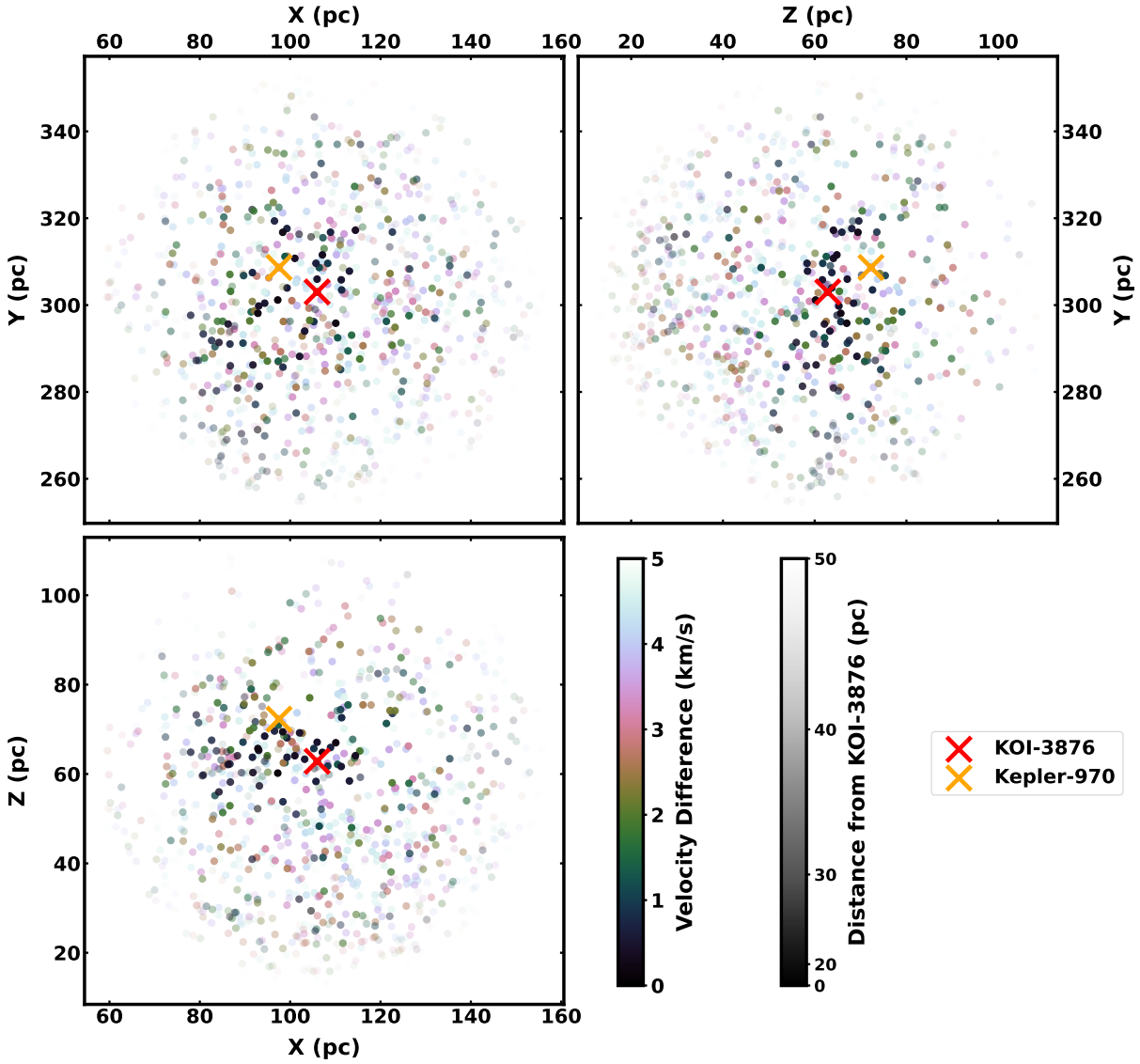

Figure 6. needs a caption here. Galactic Heliocentric (XYZ) coordinates of stars within 50pc and 5km/s of KOI-3876(marked as a red X). Kepler-970 is shown in orange. Other colors indicate the velocity difference from KOI-3876, and the transparency indicates distance from KOI-3876.

a mix of populations (e.g., binaries, field interlopers, and stars with erroneous parallaxes or photometry). The fit included six free parameters: the association age (age), the average reddening across the association ($E(B-V)$), the amplitude of the outlier population (P_B), the offset of the outlier population from the main population CMD (Y_B [mags]), the variance of the outliers around the mean (V_B [mags]), and a term to capture missing uncertainties or differential reddening across the association (f [mags]).

Reddening was limited to < 0.2 mag based on the three-dimensional extinction map from Green et al. (2019). Other parameters evolved under uniform priors, bounded only by physical limits. We re-sampled the model grid to ensure uniform distribution around the expected age (50-250 Myr).

*G*aia photometry was the only available for all targets, and was generally far more precise than other data available. Many stars were also resolved as binaries (or the target and a background star) in *G*aia, but seen as a single source in 2MASS and KIC photometry (Brown et al. 2011). So we restricted our analysis to *G*aia magnitudes.

We expect most of the initial sample of 1007 candidate members to be field interlopers (see Section 4.2). While the mixture model can handle high contamination rates by making P_B larger, tests suggest that when $P_B > 0.5$, the model will begin to call stars in the main population outliers and fit the background population as the true one (yielding a field age). To avoid this, we limited the input list to stars within 30 pc and 3km s^{-1} from KOI-3876 in three-dimensional distance and tangential velocity. We also removed any stars with a Renormalised Unit Weight Error (RUWE; Gaia Collaboration et al. 2021) > 1.2. As discussed in Ziegler et al. (2020) and Wood et al. (2021), stars above this limit are likely to be binaries. Lastly, we removed any stars that were outside the model grid range based on their absolute magnitude and/or color and stars with poor photometry or parallaxes (SNR<20). This left only 78 stars, but this was more than sufficient for a fit.

As we show in Figure 7, the resulting fit yielded an age of 104^{+8}_{-5} Myr. As a test of the systematic errors, we ran a similar fit using models from the Dartmouth Stellar Evolution Program (DSEP, Dotter et al. 2008) with magnetic enhancement described in Feiden & Chaboyer (2012). The DSEP-magnetic model fit gave a similar age of 110±11 Myr. The DSEP magnetic models did somewhat better for the low-mass stars, and yielded a more conservative uncertainty, so we adopted this as the isochronal age.

4.5. *Contamination Rate*

Based on a qualitative inspection of the proper motion and XYZ positions (see Figures 5 and 6), we expect many of our 1007 candidate members are field interlopers. We can make a more quantitative estimate of the contamination rate using our rotation and radial velocity measurements. These are particularly effective because neither was used in our initial sample selection (FriendFinder only used the velocity of KOI-3876).

We estimate the contamination rate from the ratio of the number of stars with rotation periods consistent with the Pleiades sequence compared to the total number of stars *for which we could estimate a reliable rotation period*. The importance of the cut to the ratio denominator can be seen in the M dwarfs in Figure 4; although late-type stars likely make up most of the group,

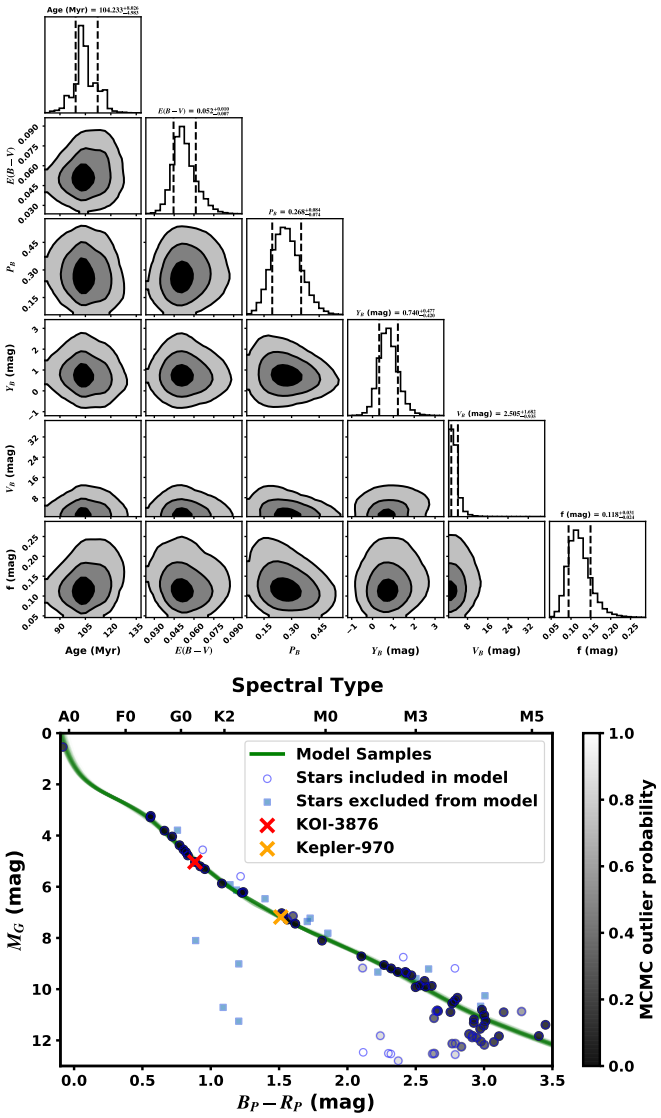

Figure 7. Comparison of the PARCSEC model isochrones to candidate members of MELANGE-2. The top shows the corner plot of our MCMC mixture model comparison, with contours corresponding to 1σ, 2σ, and 3σ. The bottom plot shows the *G*aia G versus $G - R_P$ CMD of stars included in the MCMC (blue circles) and those excluded (blue squares) due to their RUWE, color, or magnitude. Each included point is shaded based on their average outlier probability as determined by the MCMC. Many of those flagged as outliers may be non-members or members that do not follow the sequence (e.g., binaries). KOI-3876 and Kepler-970 are shown as red and orange stars. Both have low (< 4%) outlier probabilities. The green lines are 200 PARSEC isochrones with parameters drawn (randomly) from the MCMC posterior.

we have scant rotation periods past M0 simply because those stars are too faint to extract a reliable rotation curve. The few we have are mostly from *TESS*. Instead, we focus on the XXX stars with $0.4 < G - R_P < 0.8$,

which approximately corresponds to FX to KY. All stars within this range have *TESS* magnitude <, which is sufficient for extracting a usable light curve from *TESS* or *Kepler*. Of these XXX stars, YYY have rotation periods consistent with Pleiades. This suggests about ZZ% of candidate members are true members.

Our contamination estimate does not account for stars where the rotation periods are consistent with $\lesssim$100 Myr by chance. Roughly, assuming field stars are uniformly distributed from 0–10 Gyr, the number of candidates matching by chance should be $\lesssim$1. A more significant problem would be tight binaries, where the inferred rotation periods would be fast due to tidal locking or the star spun down at a slower than normal rate due to the influence of the companion. We may also miss a small number of stars due to low spot modulation, although past rotation period surveys suggest this is $< 10\%$ (e.g., Rebull et al. 2016; Douglas et al. 2017, 2019).

We can do a similar test with the radial velocities, comparing the number of stars with velocities consistent with the group

5. SEARCH FOR PLANETS IN MELANGE-2

did you use notch and locor, or just notch? To check for other candidate planets or eclipsing binaries in the same association we searched the 265 *Kepler* and *TESS* light curves using the Notch pipeline. The details of both pipelines are described in more detail in Rizzuto et al. (2017). To briefly summarize, the Notch filter fits a window of the lightcurve as a combination of an outlier-robust second-order polynomial (for the stellar variability) and a trapezoidal notch (representing the potential planet). The window moves along the lightcurve until the variability is detrended while preserving the planet signal. At each data point, we calculate the improvement from adding the trapezoidal notch based on the change in the in Bayesian Information Criterion (BIC) compared to modelling just a polynomial. LOCoR (Locally Optimized Combination of Rotations), instead models the stellar variability using linear combinations of pseudo-rotation measurements in other parts of the light curve than the region being modeled. It then repeats this process over the full curve.

We searched the detrended light curves (both Notch and LOCoR detrended) and the BIC signals that Notch produces for periodic signals. We excluded the rotation period (and aliases) of the star, as it is common to have imperfect detrending with both algorithms. In addition to our search, a number of known *Kepler* objects of interest (KOIs) reside within candidate members of MELANGE-2, identified by a simple cross-match against the most recent KOI catalog (Twicken et al. 2016).

In total, we identified 18 targets of interest that are either KOIs and/or pass the SNR and initial quality checks from Notch/LOCor. Eight of these are known KOIs (KOI-678.01, KOI-678.02, KOI-966.01, KOI-966.02, KOI-1838.01, KOI-5304.01, KOI-6819.01, and KOI-7059.01), while the remaining are newly identified.

All 18 targets are listed in Table 2 along with our classification of each. Other than KOI-3876 b, we concluded only one other detection (Kepler-970 b) was both a real planet and a member of MELANGE-2. We discuss each system and our reasons for rejection them below.

5.1. *Discussion of individual candidates*

KOI-678 (.01 and .02) contains two confirmed planets (Kepler-211 bc), and the star's light curve showed a clear rotation signature of $\simeq$13.7 days. However, this period is too long for membership given its *G*aia colors (should be $\lesssim$8 days). Similarly, the lithium equivalent width is only 3.8$m\mathring{A}$ (Berger et al. 2018), but membership would suggest a Li level above 100$m\mathring{A}$. The star's proper motion also puts it on the outskirts of the distribution. We conclude this target is unlikely to be a member.

Both planet candidates in KOI-966 are flagged as false positives by the *Kepler* analysis (Coughlin et al. 2016), with both signals attributed to an eclipsing binary (.02 corresponding to an alias of the secondary eclipse). We similarly concluded that the signal is likely an eclipsing binary based on the V-shaped transit and secondary eclipse. The star's rotation period (3.92 days; Walkowicz & Basri 2013) is consistent with membership for an M dwarf and does not match the eclipse period (0.379 days). The star is also only 1km s^{-1} and 8 pc from KOI-3876, near the core of likely members. We conclude it is likely an eclipsing binary in the association.

KOI-1838.01 is a confirmed planet (Kepler-970 b; Morton et al. 2016). The star's rotation (9.23 days) places it right on the Pleiades sequence, and much faster than the stalling regime seen for $>$ 600 Myr systems (Curtis et al. 2019). The LAMOST (corrected) velocity is -32$\pm$4 km s^{-1}, which is consistent with the value predicted for membership ($\simeq$-27km s^{-1}). A more precise measurement from the CKS-cool project Petigura (in prep) yielded an RV of -27.15$\pm$0.10km s^{-1}, an excellent match for the association. The corresponding high-resolution spectrum from Petigura (in prep) shows weak lithium ($< 40m\mathring{A}$), but this is consistent with 100 Myr for its spectral type CITE A MODEL. As we show in Figure 1, Kepler-970 lands on the expected sequence for a Pleiades-aged star. We conclude that this planet is real

and a member and include it in our analysis through the rest of the paper.

KOI-5304.01 was flagged as a false positive by the *Kepler* analysis due to a non-transit-like shape. Our visual inspection of the candidate agrees with this. The host star also shows a measurable but slow rotation period of ≃11.4 days, which is slower than expected for membership (see Section 4.2). We conclude that this is a false positive and not a member.

KOI-6819 contains a planet candidate (.01). The star shows no significant rotation, suggesting the star is of older age. The *G*aia DR2 velocity for KOI-6819 is 3.27km s^{-1}, ≃20km s^{-1} from the association. We conclude this target is unlikely to be a member.

KOI-7059.01 is flagged as a false positive by the *Kepler* analysis (Coughlin et al. 2016), and the odd-even depth difference strongly suggests and eclipsing binary. The APOGEE velocity is ≃8km s^{-1} from the cluster. The discrepant velocity may be due to binarity, but the source also lands on the outskirts of the membership list, >48 pc from KOI-3876 and near the edge in terms of tangential velocity. We conclude this target is likely a real eclipsing binary and unlikely to be a member.

For the newly identified targets, KICs 1137886, 6134939, 6366739, 6589221, 9139566, and 9700914 and TICs 164461070, 20352534, 272486188, 273383615, 28768382, and 355909811, were all ultimately rejected based on their transit signals. For most cases, this was determined by the BIC score computed by the Notch filter search; all but two had BIC scores was below our threshold of significance. Visual inspection of each confirmed this rejection. The other two, KIC 9700914 and KIC 6589221, both showed potentially interesting signatures in the *TESS* data (Figure 8). However, we failed to recover the transit signal in the higher-quality *Kepler* data.

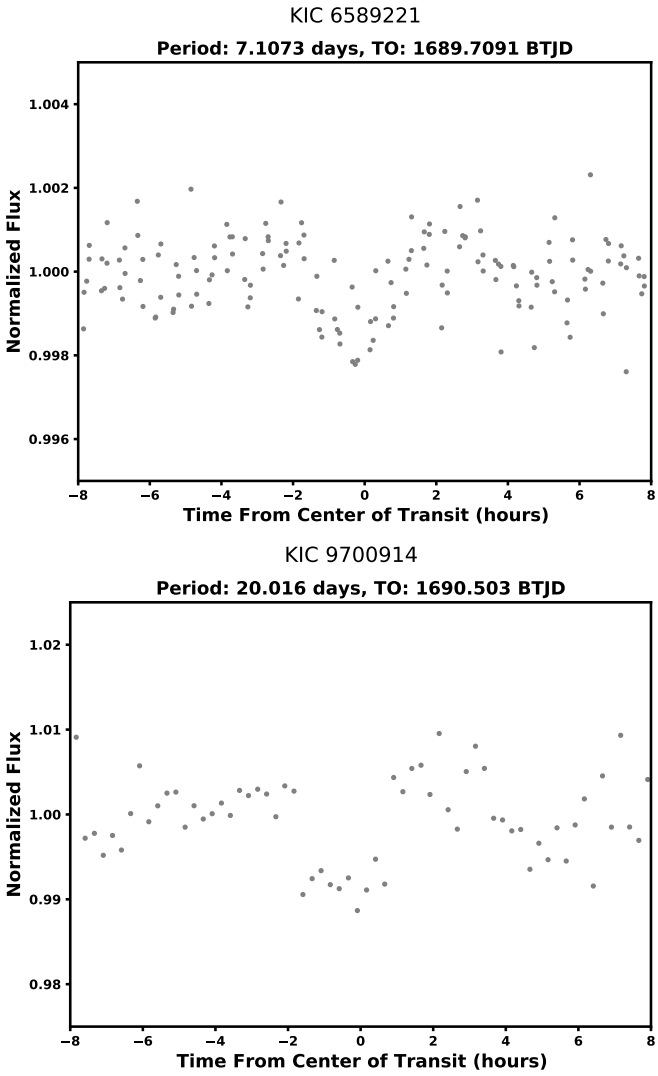

Figure 8. Phase-folded light curve of potential member KIC 6589221 from *TESS* detrended with Notch and LOCoR (grey points). We find that the best fit period is 7.1073 days, with an initial transit time of 1689.709 BTJD.

6. PARAMETERS OF THE PLANET HOSTS

We summarize constraints on both host stars in Table 3, the details of which we provide below.

6.1. *Literature Parameters*

As a reasonably bright (K_P = 12.6) star hosting a planet candidate from the *Kepler* mission, KOI-3876 has numerous stellar parameters in the literature. The California *Kepler* Survey (CKS) estimate $T_{\rm eff}$=5720 ± 60 K, *log g* =4.64±0.1, and $v \sin i_*$=9.9±1.0km s^{-1}, $R_*0.95^{+0.06}_{-0.04}R_\odot$ and M_* = 1.01 ± 0.03$M_\odot$ based on comparing their high-resolution spectra and comparison to well-characterized templates (Petigura et al. 2017; Yee et al. 2017) and stellar isochrones (Johnson et al. 2017). Brewer & Fischer (2018), using the same spectra, estimate $T_{\rm eff}$=5642±27 K, *log g* =4.46±0.05, R_* = 0.93 ± 0.02$M_\odot$, M_* = 0.99 ± 0.02$M_\odot$, and $v \sin i_*$=10.4±0.5km s^{-1}, as well as detailed abundances that are generally consistent with the Solar value. Berger et al. (2020) incorporated *G*aia DR2 data with MIST stellar isochrones to derive an $T_{\rm eff}$=5577 ± 85 K, *log g* = 4.50 ± 0.02, and R_* = 0.908 ± 0.017$R_\odot$.

For Kepler-970, Berger et al. (2020) estimated $T_{\rm eff}$=4314±73 K, *log g* = 4.63 ± 0.02, R_* = 0.649 ± 0.012$R_\odot$, and M_* = 0.657 ± 0.022$M_\odot$ using the *G*aia parallax, photometry, and MIST isochrones as with KOI-3876. Based on the CKS spectra, Petigura (in prep) found a consistent $T_{\rm eff}$ (4401±70 K), stellar ra-

Table 2. Planetary Candidates in MELANGE-2.

ID	Disposition	Probable Member?	Period (days)	T0 (BJD)	Approximate Depth (ppm)
KOI-678.01	Confirmed	N	6.040	2455005.594	240.999
KOI-678.02	Confirmed	N	4.139	2454965.016	256.500
KOI-966.01	EB	Y	0.379	2455003.248	1973.300
KOI-966.02	EB	Y	7.769	2454966.090	
KOI-1838.01	Confirmed	Y	16.736	2454976.132	1147.000
KOI-5304.01	FP	N	206.310	2455064.818	277.099
KOI-6819.01	Candidate	N	3.226	2454967.419	36.300
KOI-7059.01	EB	N	31.973	2454966.867	75053.699
KIC 1137886	Candidate		10.870	2458690.562	3178.200
KIC 6134939	Candidate		19.701	2458687.657	1858.542
KIC 6366739	Candidate		22.321	2455386.607	2277.944
KIC 6589221	Candidate	Y	7.107	2458689.709	1908.620
KIC 9139566	Candidate	N	12.392	2458695.552	1277.229
KIC 9700914	Candidate	N	20.016	2458690.503	400.041
TIC 164461070	Candidate				
TIC 20352534	Candidate	N	6.377	2458687.871	5852.463
TIC 272486188	Candidate	N	9.040	2458683.604	779.379
TIC 273383615	Candidate				
TIC 28768382	Candidate	N	11.790	2458692.723	1430.802
TIC 355909811	Candidate		6.065	2458686.931	34080.851

dius ($R_* = 0.70 \pm 0.03 R_\odot$), and mass ($M_* = 0.68 \pm 0.10 M_\odot$). Petigura (in prep) also estimated a $v \sin i_*$ of 5.21±1.0km s^{-1} from the CKS spectra. This $v \sin i_*$ may be slightly overestimated due to mild broadening in their templates, but the errors are sufficiently generous for our analysis.

These stellar parameters are generally in agreement with each other. However, those that relied on isochrones (e.g., Berger et al. 2020) assigned > 2 Gyr ages for both stars, much older than the true $\simeq$100 Myr age from the association. Although the assigned age errors were large, the derived parameters may still be biased by the lack of an assigned age. Although this will not impact purely spectroscopic parameters like $T_{\rm eff}$ and $v \sin i_*$, the assumption can have a strong impact on the estimated stellar mass. Thus, we revisit these parameters with our own analysis below.

6.2. *Spectral-Energy Distribution*

We fit the observed spectral-energy-distribution (SED) of both stars following Mann et al. (2016a). To briefly summarize, we fit the observed photometry with a grid of optical and near-infrared flux-calibrated spectra spanning 0.4–2.3μm. We included BT-SETTL CIFIST atmospheric models (Baraffe et al. 2015) in the fit, both to estimate the $T_{\rm eff}$ and fill in gaps in the template spectra (e.g., beyond 2.3μm). We integrated the resulting absolutely-calibrated spectrum to estimate the bolometric flux ($F_{\rm bol}$), which we combined with the *G*aia EDR3 parallax to estimate the stellar luminosity (L_*). With $T_{\rm eff}$ and L_*, we calculated R_* using the Stefan-Boltzmann relation. While reddening in this sight-line is low (Schlafly & Finkbeiner 2011), KOI-3876 is well outside the Local Bubble, so we included extinction as part of the fit. To account for variability in the star, we added (in quadrature) 0.02 mags to the errors of all optical photometry. In total, the fit included six free parameters: the spectral template, A_V, three parameters that describe the model (log g, $T_{\rm eff}$, and [M/H]), and a scale factor between the model and the photometry. We show an example fit in Figure 9.

For KOI-3876, the resulting fit yielded $A_V = 0.16^{+0.10}_{-0.08}$, $T_{\rm eff}$=5672 ± 65 K, $F_{\rm bol}$=(2.55 ± 0.10) × 10^{-10} (erg cm^{-2} s^{-1}), L_*=0.81 ± 0.03$L_\odot$, and $R_* = 0.94 = 0.03 R_\odot$. For Kepler-970, we found $A_V = 0.28 \pm 0.12$, $T_{\rm eff}$=4290 ± 70 K, $F_{\rm bol}$=(4.88 ± 0.23) × 10^{-11} (erg cm^{-2} s^{-1}), $L_* = 0.168 \pm 0.010 L_\odot$, and $R_* = 0.715 \pm 0.03 R_\odot$.

Our SED parameters were in good agreement with the literature spectroscopic values for both stars. Since KOI-3876 is Sun-like, we considered the high-resolution spectroscopic $T_{\rm eff}$ to be more reliable than the SED-based value, but the SED-based luminosity (and radius) more reliable than one derived from the spectroscopic *log g* or isochrone. We combined the two, which yielded a final radius of $0.92 \pm 0.02 R_\odot$. For Kepler-970, we adopted our SED-fit parameters for all values.

6.3. *Stellar mass*

To determine M_* for KOI-3876, we compared the observed photometry to Solar-metallicity magnetic DSEP evolution models and PARSEC models. We used `emcee`

to simultaneously fit for age, A_V, M_*, and an additional parameter to capture underestimated uncertainties in the data or models (f, in magnitudes) within an MCMC framework. We used a hybrid interpolation method, first identifying the nearest age in then model grid and then performing a linear interpolation in mass to obtain stellar parameters and model photometry. Since this method could not interpolate between ages, we re-sampled the input grid using the `isochrones` package (Morton 2015a) to be more dense (0.1 Myr and $0.01 M_\odot$) than expected errors. To redden the model photometry, we used `synphot` (Lim 2020) and the extinction law from Cardelli et al. (1989). We placed a Gaussian prior on age of 110±11 Myr, while other parameters evolved under uniform priors. The resulting fit from each model grid was very precise, but differences between the two grids suggest larger systematic errors. Considering these, the resulting parameters were generally in agreement with our spectroscopic constraints ($R_* = 0.968 \pm 0.07$, $A_V = 0.27 \pm 0.10$, $T_{\rm eff}$=5710±60) and provided a stellar mass estimate of $M_* = 1.04 \pm 0.03 M_\odot$. We combined this with our earlier radius estimate to get an estimate of the stellar density ($\rho_* = 1.30 \pm 0.10 \rho_o dot$).

Kepler-970 is low-mass enough to fit within the bounds of the $M_K - M_*$ relation from Mann et al. (2019). We used the *G*aia EDR3 parallax with uncertainties corrected for underestimated errors following El-Badry et al. (2021) and the 2MASS K_S magnitude. We applied a correction for reddening based on our SED fit (Section 6.2), although this was negligible in K_S band compared to other uncertainties. We fed the resulting values into the fit posteriors using the provided code[3], which yielded a mass of $0.66 \pm 0.02 M_\odot$. Combining with the radius above, this gives a stellar density of $1.88 \pm 0.24 \rho_\odot$.

6.4. *Stellar inclination*

To test whether the stellar spin and planetary orbit are consistent with alignment, we computed the stellar inclination (i_*) from the $v \sin i_*$, $P_{\rm rot}$, and R_* values estimated above. In is simplest form, this calculation is $V = 2\pi R_* / P_{\rm rot}$, but requires additional statistical corrections (see Morton & Winn 2014; Masuda & Winn 2020). Here we followed the methodology described in Masuda & Winn (2020). For KOI-3876, the resulting stellar inclination was $i_* > 71°$ at 95% confidence and $i_* > 80°$ at 68% confidence. For Kepler-970, the values were $i_* > 52°$ and $i_* > 70°$ at 95% and 68%, respectively. Both are consistent with alignment with the orbital inclinations.

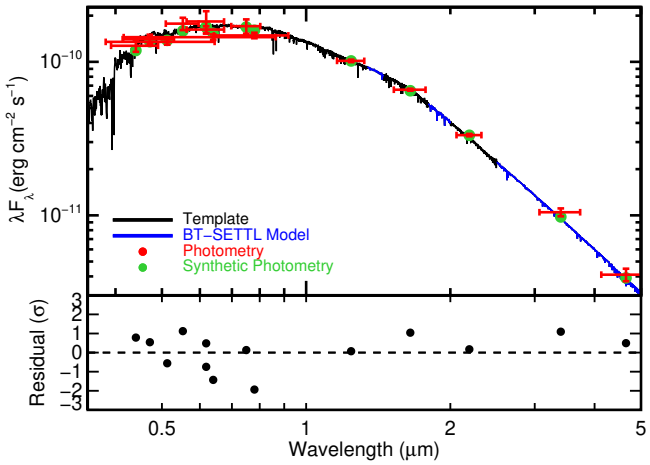

Figure 9. Best-fit template spectrum (G1V; black) and synthetic photometry (green) compared to the observed photometry of KOI-3876 (red). Errors on observed photometry are shown as vertical error bars, while horizontal error bars indicate the approximate width of the filter. BT-SETTL models (blue) were used to fill in regions of high telluric absorption or beyond the template range. The bottom panel shows the photometric residual in units of standard deviations.

7. TRANSIT PARAMETERS

We fit the *Kepler* photometry using the `misttborn` (MCMC Interface for Synthesis of Transits, Tomography, Binaries, and Others of a Relevant Nature) fitting code[4] first described in Mann et al. (2016b) and expanded upon in Johnson et al. (2018). `misttborn` uses `BATMAN` (Kreidberg 2015) to generate model light curves and `emcee` (Foreman-Mackey et al. 2013) to explore the transit parameter space.

The standard implementation of `misttborn` fits for six parameters for each transiting planet: time of periastron (T_0), orbital period of the planet (P), planet-to-star radius ratio ($R_p/R_\star$), impact parameter (b), and stellar density ($\rho_\star$). We fit two linear and quadratic limb-darkening coefficients (q_1, q_2) following the triangular sampling prescription of Kipping (2013).

We ran two versions of the fit. In the first, the MCMC chain restricted e to 0 and allowed $\rho_\star$ to vary within a uniform distribution, and the second allowed e to vary with a Gaussian prior on $\rho_\star$ from our spectroscopic and SED analysis (Section 6). For both fits, applied Gaussian priors on the limb-darkening coefficients based on the values derived using our stellar parameters from Sec-

[3] https://github.com/awmann/M_-M_K-

[4] https://github.com/captain-exoplanet/misttborn

Table 3. Properties of KOI-3876 and Kepler-970

Parameter	KOI-3876	Kepler-970	Source
		Name	
Gaia EDR3	2052827207364859264	2101379205604338688	Gaia Collaboration et al. (2021)
KOI	3876	1838	Twicken et al. (2016)
KIC	3440118	5526527	Brown et al. (2011)
TIC	122450696	122069243	Stassun et al. (2018)
2MASS	J19214575+3831248	J19183005+4042314	Skrutskie et al. (2006)
		Astrometry	
α	290.440629	289.625218	*Gaia* EDR3
δ.	38.523572	40.708735	*Gaia* EDR3
μ_α (mas yr^{-1})	-4.154±0.010	-2.739±0.020	*Gaia* EDR3
μ_δ (mas yr^{-1})	2.269±0.011	1.652±.024	*Gaia* EDR3
π (mas)	3.0565±0.0093	3.0153±0.0186	*Gaia* EDR3
		Photometry	
G_{Gaia} (mag)	12.6054±0.0028	14.7876±0.0029	*Gaia* EDR3
BP_{Gaia} (mag)	12.9642±0.0033	5.4884±0.0049	*Gaia* EDR3
RP_{Gaia} (mag)	12.0798±0.0041	13.9759±0.0048	*Gaia* EDR3
B (mag)	13.375 ± 0.094	...	APASS
V (mag)	12.655 ± 0.122	...	APASS
g' (mag)	13.038 ± 0.033	...	APASS
r' (mag)	12.456 ± 0.092	...	APASS
i' (mag)	12.323 ± 0.062	...	APASS
J (mag)	11.456 ± 0.02	12.980±0.023	2MASS
H (mag)	11.152 ± 0.016	12.355±0.023	2MASS
K_S (mag)	11.107 ± 0.019	12.215±0.022	2MASS
$W1$ (mag)	11.06 ± 0.023	12.155±0.022	ALLWISE
$W2$ (mag)	11.09 ± 0.020	12.193±0.022	ALLWISE
$W3$ (mag)	10.91 ± 0.094	12.195±0.282	ALLWISE
		Kinematics & Position	
RV_{Bary} (km s^{-1})	-26.79±0.01	-27.15±0.10	Jönsson et al. (2020); Petigura (in prep)
U (km s^{-1})	-9.467 ± 0.016	-8.815 ± 0.047	This work
V (km s^{-1})	-26.034 ± 0.012	-26.146 ± 0.092	This work
W (km s^{-1})	2.048 ± 0.032	-1.034 ± 0.055	This work
X (pc)	105.98 ± 0.42	97.55 ± 0.78	This work
Y (pc)	303.03 ± 1.20	308.66 ± 2.45	This work
Z (pc)	62.86 ± 0.25	72.28 ± 0.58	This work
		Physical Properties	
P_{rot} (days)	4.69 ± 0.04	9.23 ±0.66	Nielsen et al. (2013); Santos et al. (2019)
$v \sin i_*$ (km s^{-1})	10.4 ± 0.5	5.2±1.0km s^{-1}	Brewer & Fischer (2018); Petigura (in prep)
i_* (°)	> 80	> 52	This work
F_{bol} (erg cm^{-2} s^{-1})	(2.55 ± 0.10) × 10^{-10}	(4.88 ± 0.23) × 10^{-11}	This work
T_{eff} (K)	5720 ± 60	4290 ± 70	CKS; This work
[Fe/H]	0.12 ± 0.02	0.04±0.09	Brewer & Fischer (2018); Petigura (in prep)
$M_\star$ ($M_\odot$)	1.01 ± 0.03	0.67±0.02	This work
$R_\star$ ($R_\odot$)	0.92 ± 0.02	0.71 ± 0.03	This work
$L_\star$ ($L_\odot$)	0.81 ± 0.03	0.168 ± 0.010	This work
$\rho_\star$ ($\rho_\odot$)	1.30 ± 0.10	1.88±0.24	This work
Age (Myr)	110 ± 11		This work

tion 6 and the `LDTK` toolkit Parviainen & Aigrain (2015), with errors accounting for the difference between models: $g_1 = 0.42 \pm 0.08$, $g_2 = 0.13 \pm 0.04$ for KOI3876 and $g_1 = 0.51 \pm 0.08$, $g_2 = 0.13 \pm 0.04$ for Kepler-970. Other transit parameters were sampled uniformly with physically motivated boundaries; e.g., T_0 was restricted to the time period sampled by the data, $|b| < 1 + R_P/R_*$, $0 < e < 1$, $0 < \rho_*$, and $0 < R_P/R_* < 1$.

To model stellar variations, `misttborn` includes a Gaussian Process (GP) regression module, utilizing the `celerite` code (Foreman-Mackey et al. 2017). We used a mixture of two stochastically driven damped simple harmonic oscillators (SHOs) at periods P_{GP} (primary) and $0.5P_{GP}$ (secondary). In total, there were five GP parameters: the log of the dominant period ($\ln(P_{GP})$), the log of the GP amplitude (ln Amp), a decay timescale

for the variability (quality factor, $\ln Q0$), the difference between the primary and secondary quality factors ($\ln \Delta Q$), and a mix parameter that describes how the primary and secondary signals are combined (Mix). We used a weak Gaussian prior (assuming 20% errors) on the GP period to keep walkers from wandering to half and double aliases. All GP parameters evolved under uniform priors.

For each of four runs (two planets each with and without eccentricity), we ran the MCMC using 50 walkers for 250000 steps including a burn-in of 20000 steps. The total run was more than 50 times the autocorrelation time (for all fits), indicating that the total run was sufficient for convergence.

As we show in Figures 10, the SHOs GP did an excellent job describing the overall variability for both planets, even in the presence of complex changes in the light curve morphology over 4.5 years of observations by *Kepler*. We also show the phase folded light curves in Figure 11 for the fit where e was allowed to vary. The best-fit parameters with uncertainties for both fits can be found in Table 4, and the corner plot for the major transit-fit parameters for the eccentric fit is in Figure 12.

Update for 2nd star The first fit ($e = 0$) yields a $\rho_\star$ value much larger than the spectroscopic/isochronal value determined in Section 6 ($15.5\rho_\odot$ vs $1.3\rho_\odot$). Although the error on the transit-fit density is large ($5.9\rho_\odot$), so the two values are consistent at $\simeq 2.5\sigma$. But this suggests the planet is likely to be eccentric. Indeed, in the fit where e is allowed to float, the preferred e is 0.2–0.4. For this reason, we adopt the second fit, where e is allowed to float, as the preferred fit.

7.1. *False Positive Analysis*

In Morton et al. (2016), the authors run the false-positive probability calculator `VESPA` Morton (2015b) on all *Kepler* objects of interest available at the time, which included KOI-3876 b. They assigned a high probability that KOI-3876 b (90%) that KOI-3876 b is an eclipsing binary, and $< 1\%$ that the signal is due to a planet overall. This conclusion was based primarily on the light curve morphology and available stellar parameters.

As we show in Figure 13, radial velocities from the Apache Point Observatory Galactic Evolution Experiment 16th data release (APOGEE DR16; Jönsson et al. 2020) rule out any stellar companion at the period of the planet. Further, our light curve analysis shows the expected U-shape transit for a planet, and there is no sign of a companion in the extant spectroscopy or adaptive optics imaging and non-redunant aperture masking from Kraus et al. (2016). *G*aia EDR3 astrometry and imaging similarly shows no sign of a companion. There is only one star detected with the *Kepler* PSF, which is too faint to reproduce the transit.

KOI-3876 also has a low Renormalised Unit Weight Error (RUWE) in EDR3 (0.94)

RUWE value is effectively an astrometric reduced χ^2 value, normalized to correct for color and brightness dependent effects[5]. RUWE should be around 1 for well-behaved sources, and higher values (RUWE$\gtrsim$1.3) suggests with the presence of a stellar companion (Ziegler et al. 2020; Wood et al. 2021).

It is possible the high Morton et al. (2016) was an artifact of poor detrending of the high stellar variability in KOI-3876 and/or the mismatch between the transit duration and that expected for a circular orbit (see Section 7). This motivated a

Rerunning the `VESPA` analysis, we find a 97% probability KOI-3876 b is a planet and a 3% probability KOI-3876 b is an eclipsing binary. As previously stated, shown in Figure 13, a stellar companion to KOI-3876 is ruled out at the period of the planet. Therefore, we conclude KOI-3876 b is a planet.

AWM: do we want to say something about the AO imaging somewhere.

8. SUMMARY AND CONCLUSIONS

KOI-3876 b is a $\simeq$ 110 Myr planet in the newly identified MELANGE-2 association. KOI-3876 b is about twice the size of the earth, orbiting a star that is a young analog to the Sun, having a similar radius and mass. Originally flagged as a false positive by //false positive work//, we rule out this disposition based on APOGEE radial velocities and our own light curve analysis. We see that the radial velocity dispersion of the system is not well-modeled by a stellar-mass body, ruling out the possibility of an eclipsing binary. The scatter in radial velocity is likely due to the stellar jitter that is common in young stars since the variation is still below expected for even a tight eclipsing binary.

We used rotation periods, lithium, and isochronal evolution models in order to age MELANGE-2 and thus KOI-3876 b to 110 ± 10 Myr. Based on //theia work//, we conclude that MELANGE-2may(not) be a subgroup of the larger Theia 316 association. //Theia 316 conclusion// Due to the high number of stars too faint for

[5] https://gea.esac.esa.int/archive/documentation/GDR2/Gaia_archive/chap_datamodel/sec_dm_main_tables/ssec_dm_ruwe.html

Table 4. Parameters of KOI-3876and Kepler-970

Parameter	KOI-3876		Kepler-970	
	e=0	e float (preferred)	e=0	e float (preferred)
Measured Parameters				
T_0 (BJD-2454833)	131.71494 ± 0.00087	$131.71488^{+0.00089}_{-0.0009}$	$143.13254^{+0.00098}_{-0.00096}$	
P (days)	$19.577829 \pm 2.1 \times 10^{-5}$	$19.57783^{+2.2\times10^{-5}}_{-2.3\times10^{-5}}$	$16.736525 \pm 2 \times 10^{-5}$	
$R_P/R_\star$	$0.01946^{+0.00061}_{-0.00043}$	$0.02112^{+0.00092}_{-0.00079}$	$0.03292^{+0.00115}_{-0.00098}$	
b	$0.31^{+0.28}_{-0.22}$	$0.803^{+0.081}_{-0.1}$	$0.59^{+0.16}_{-0.18}$	
$\rho_\star$ ($\rho_\odot$)	$15.5^{+2.5}_{-5.9}$	$1.308^{+0.09}_{-0.089}$	9.9 ± 4.5	
$q_{1,1}$	$0.291^{+0.107}_{-0.099}$	$0.305^{+0.101}_{-0.096}$	$0.33^{+0.27}_{-0.2}$	
$q_{2,1}$	$0.371^{+0.075}_{-0.086}$	$0.373^{+0.077}_{-0.09}$	$0.23^{+0.15}_{-0.14}$	
$\sqrt{e}\sin\omega$	–	$0.29^{+0.16}_{-0.22}$	–	
$\sqrt{e}\cos\omega$	–	-0.07 ± 0.48	–	
$\log(P_{GP})$	1.5658 ± 0.0036	$2.09^{+0.012}_{-0.5}$	$3.284^{+0.026}_{-0.023}$	
$\log(Amp)$	$-9.48^{+0.13}_{-0.12}$	$-9.348^{+0.095}_{-0.2}$	$-7.264^{+0.146}_{-0.081}$	
$\log(\Delta Q)$	2.41 ± 0.22	$108.7^{+170.0}_{-110.0}$	180.0 ± 120.0	
$\log(Q0)$	$1.36^{+0.059}_{-0.056}$	$1.195^{+0.162}_{-0.08}$	$0.0056^{+0.0093}_{-0.0042}$	
$\log(Mix)$	$-1.56^{+0.16}_{-0.17}$	$3.6^{+4.2}_{-5.1}$	$5.3^{+3.2}_{-3.4}$	
Derived Parameters				
$a/R_\star$	$76.2^{+3.9}_{-10.0}$	$40.2^{+4.1}_{-4.4}$	$59.2^{+7.8}_{-10.0}$	
i (°)	$89.76^{+0.17}_{-0.29}$	$88.56^{+0.19}_{-0.13}$	$89.43^{+0.22}_{-0.32}$	
T_{14} (days)	$0.0794^{+0.0016}_{-0.0015}$	$0.097^{+0.044}_{-0.019}$	$0.0764^{+0.003}_{-0.0025}$	
T_{23} (days)	$0.0756^{+0.0015}_{-0.0016}$	$0.085^{+0.042}_{-0.02}$	$0.0684^{+0.0027}_{-0.0032}$	
a (AU)	$0.326^{+0.018}_{-0.049}$	0.165 ± 0.029	$0.195^{+0.027}_{-0.037}$	
e	...	$0.27^{+0.16}_{-0.14}$	...	
ω (°)	...	$114.0^{+55.0}_{-73.0}$	...	

radial velocity and Lithium follow-up, it is uncertain whether or not these groups overlap.

Using misttborn, we find that KOI-3876 b likely has an eccentric orbit. We find that we can only match the fitted stellar density and the estimated isochronal density by allowing the eccentricity to vary in the fit rather than fixing it to 0. Because of this, we prefer the eccentric fit parameters over the fixed eccentricity fit.

Further, we identified additional candidates in the association for future follow-up that have potential of being planetary candidates. Due to the low SNR of the targets, we simply call these candidates in need of follow up.

8.1. *Theia ???*

How many of our candidates are in Theia? Can we make a plot showing some of the overlap? Do we conclude that this means we are just looking at Theia? Note that future work should sort this out by getting spectra (RVs, lithium) and rotation for Theia to check if the group is truly co-eval.

The THYME collaboration would like to acknowledge Halee, who kept Madyson sane during lockdown. We also thank Madyson's little sister, who is probably asleep right now.

MGB was supported by the NC Space Grant Undergraduate Research program and by funding from the Chancellor's Science Scholars Program at the University of North Carolina at Chapel Hill.

AWM was supported through NASA's Astrophysics Data Analysis Program (80NSSC19K0583). MLW was supported by a grant through NASA's $K2$ GO program (80NSSC19K0097). This material is based upon work supported by the National Science Foundation Graduate Research Fellowship Program under Grant No. DGE-1650116 to PCT.

This paper includes data collected by the TESS mission, which are publicly available from the Mikulski Archive for Space Telescopes (MAST). Funding for the TESS mission is provided by NASA's Science Mission directorate. This research has made use of the Exoplanet Follow-up Observation Program website, which is operated by the California Institute of Technology, under contract with the National Aeronautics and Space Administration under the Exoplanet Exploration Program. This work has made use of data from the European Space Agency (ESA) mission *Gaia* [6], processed by the *Gaia* Data Processing and Analysis Consortium (DPAC)[7]. Funding for the DPAC has been provided by national institutions, in particular the institutions participating in the *Gaia* Multilateral Agreement. This

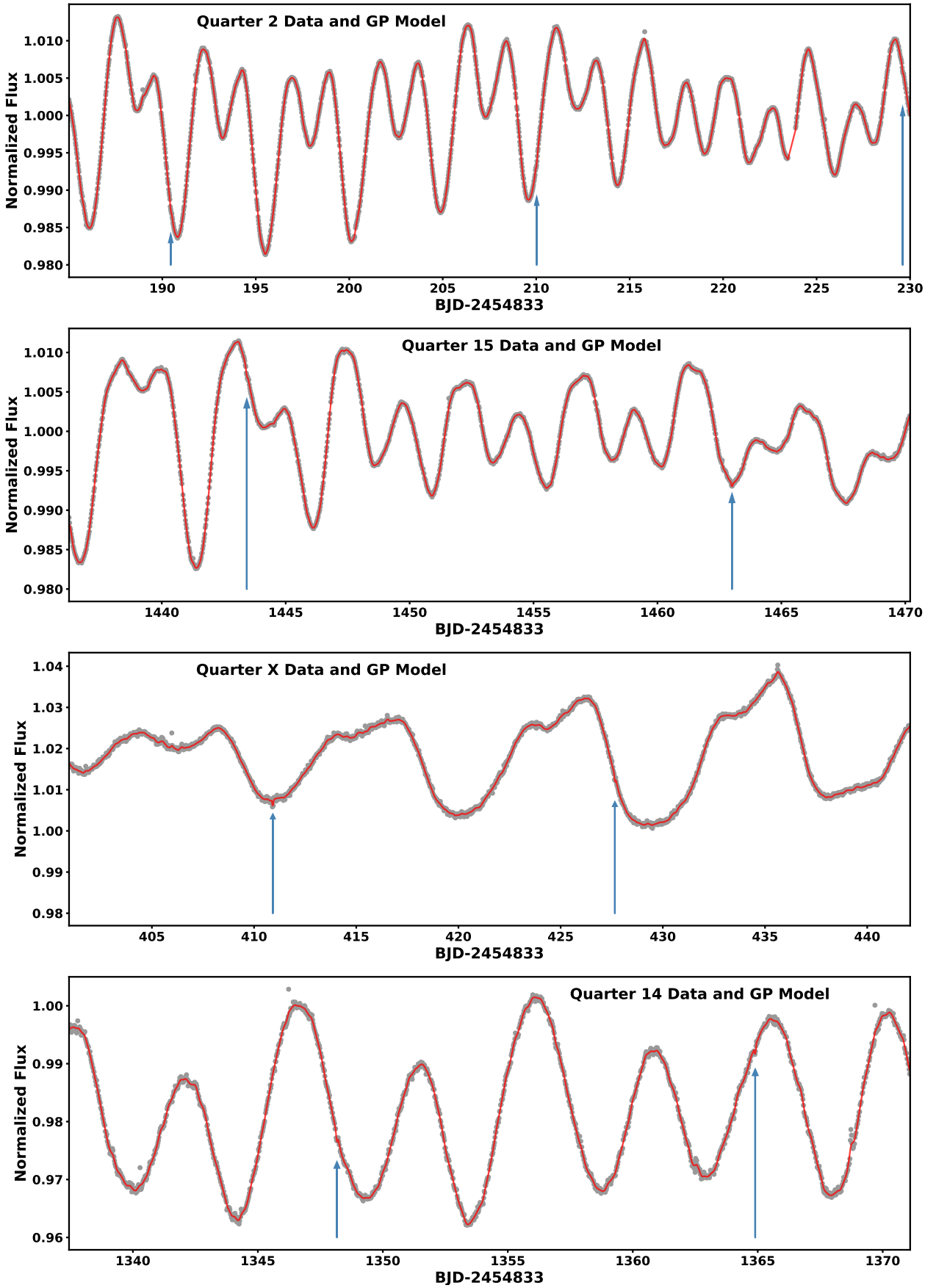

Figure 10. Approximately 40-day light curves from *Kepler* Quarters 2 (top) and 15 (2nd from top) for KOI-3876, and Quarters 4 (3rd from top) and Quarters 14 (bottom) for Kepler-970. The normalized flux (grey) is shown with our best-fit GP model (red). The locations of transits are shown with the blue arrows.

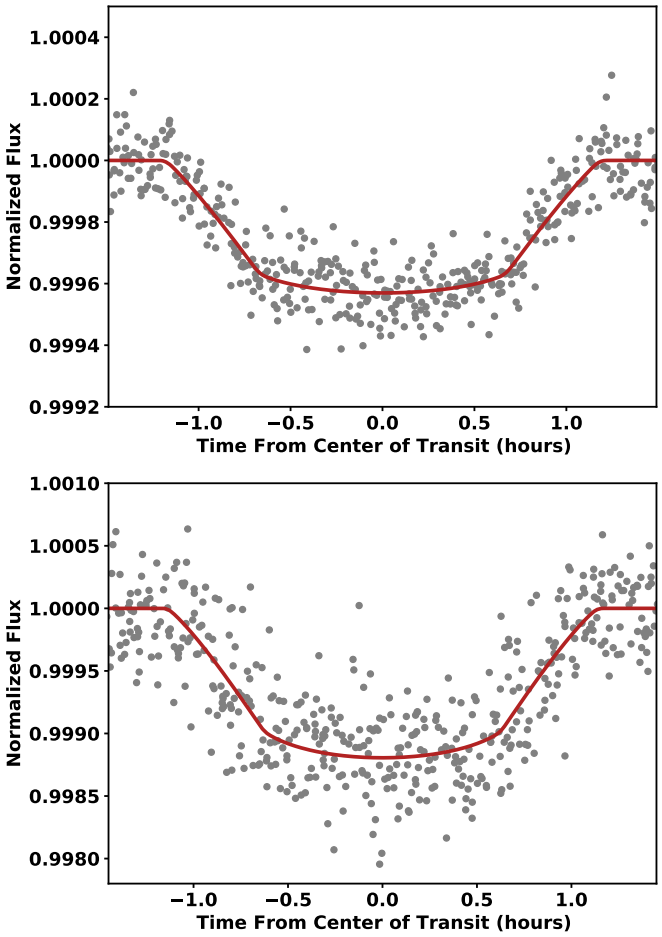

Figure 11. Phase-folded light curve of KOI-3876 (top) and Kepler-970 (bottom) from *Kepler* (grey points) with the best-fit transit model (red). The best-fit GP model to the stellar variability has been removed from both the data and the model for clarity.

Facilities: TESS, Kepler, Gaia, Smith (Coude)

Software: `misttborn.py`, *emcee* (Foreman-Mackey et al. 2013), *batman* (Kreidberg 2015), matplotlib (Hunter 2007), `corner.py` (Foreman-Mackey 2016)

REFERENCES

Aigrain, S., Llama, J., Ceillier, T., et al. 2015, MNRAS, 450, 3211, doi: 10.1093/mnras/stv853

Anguiano, B., Majewski, S. R., Allende Prieto, C., et al. 2018, A&A, 620, A76, doi: 10.1051/0004-6361/201833387

Angus, R., Aigrain, S., Foreman-Mackey, D., & McQuillan, A. 2015, MNRAS, 450, 1787, doi: 10.1093/mnras/stv423

Baraffe, I., Homeier, D., Allard, F., & Chabrier, G. 2015, A&A, 577, A42, doi: 10.1051/0004-6361/201425481

Barnes, S. A. 2007, ApJ, 669, 1167, doi: 10.1086/519295

Berger, T. A., Howard, A. W., & Boesgaard, A. M. 2018, ApJ, 855, 115, doi: 10.3847/1538-4357/aab154

Berger, T. A., Huber, D., van Saders, J. L., et al. 2020, AJ, 159, 280, doi: 10.3847/1538-3881/159/6/280

Bochanski, J. J., Munn, J. A., Hawley, S. L., et al. 2007, AJ, 134, 2418, doi: 10.1086/522053

Bouvier, J., Barrado, D., Moraux, E., et al. 2018, A&A, 613, A63, doi: 10.1051/0004-6361/201731881

Brems, S. S., Kürster, M., Trifonov, T., Reffert, S., & Quirrenbach, A. 2019, A&A, 632, A37, doi: 10.1051/0004-6361/201935520

Bressan, A., Marigo, P., Girardi, L., et al. 2012, MNRAS, 427, 127, doi: 10.1111/j.1365-2966.2012.21948.x

Brewer, J. M., & Fischer, D. A. 2018, ApJS, 237, 38, doi: 10.3847/1538-4365/aad501

Brown, T. M., Latham, D. W., Everett, M. E., & Esquerdo, G. A. 2011, AJ, 142, 112, doi: 10.1088/0004-6256/142/4/112

Cardelli, J. A., Clayton, G. C., & Mathis, J. S. 1989, ApJ, 345, 245, doi: 10.1086/167900

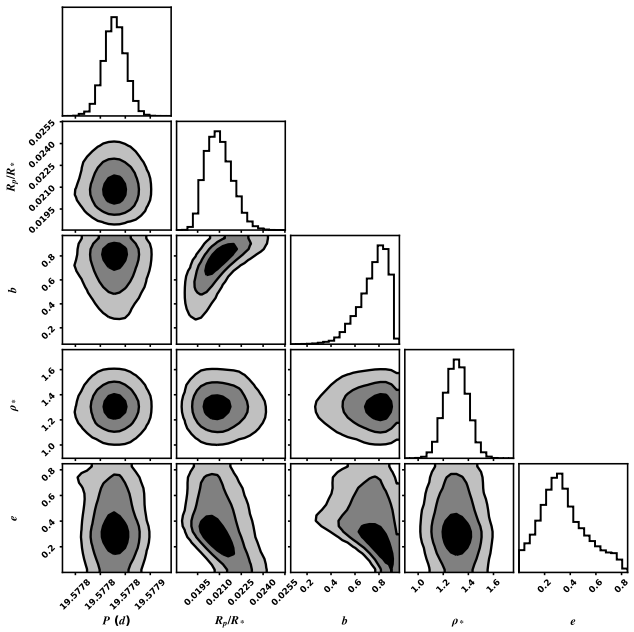

Figure 12. Corner plot of the major transit parameters (P, R_P/R_*, b, ρ_*, and e) from our `MISTTBORN` fit. The contour levels correspond to 1σ, 2σ, and 3σ of the points (from darkest to lightest). The planet-to-star radius ratio and eccentricity are strongly covariant with impact parameter, as a higher impact parameter requires a deeper transit (and lower eccentricity) to reproduce the observed transit depth (and duration). Plot made using `corner.py` (Foreman-Mackey 2016).

Corsaro, E., Stello, D., Huber, D., et al. 2012, ApJ, 757, 190, doi: 10.1088/0004-637X/757/2/190

Coughlin, J. L., Mullally, F., Thompson, S. E., et al. 2016, ApJS, 224, 12, doi: 10.3847/0067-0049/224/1/12

Cummings, J. D., Deliyannis, C. P., Maderak, R. M., & Steinhauer, A. 2017, AJ, 153, 128, doi: 10.3847/1538-3881/aa5b86

Curtis, J. L., Agüeros, M. A., Douglas, S. T., & Meibom, S. 2019, ApJ, 879, 49, doi: 10.3847/1538-4357/ab2393

Cutri, R. M., & et al. 2014, VizieR Online Data Catalog, II/328

Dotter, A., Chaboyer, B., Jevremović, D., et al. 2008, ApJS, 178, 89, doi: 10.1086/589654

Douglas, S. T., Agüeros, M. A., Covey, K. R., & Kraus, A. 2017, ApJ, 842, 83, doi: 10.3847/1538-4357/aa6e52

Douglas, S. T., Curtis, J. L., Agüeros, M. A., et al. 2019, ApJ, 879, 100, doi: 10.3847/1538-4357/ab2468

El-Badry, K., Rix, H.-W., & Heintz, T. M. 2021, MNRAS, 506, 2269, doi: 10.1093/mnras/stab323

Feiden, G. A., & Chaboyer, B. 2012, ApJ, 761, 30, doi: 10.1088/0004-637X/761/1/30

Foreman-Mackey, D. 2016, The Journal of Open Source Software, 1

Foreman-Mackey, D., Agol, E., Ambikasaran, S., & Angus, R. 2017, AJ, 154, 220, doi: 10.3847/1538-3881/aa9332

Foreman-Mackey, D., Hogg, D. W., Lang, D., & Goodman, J. 2013, PASP, 125, 306, doi: 10.1086/670067

Gagné, J., Faherty, J. K., Moranta, L., & Popinchalk, M. 2021, ApJL, 915, L29, doi: 10.3847/2041-8213/ac0e9a

Gagné, J., Mamajek, E. E., Malo, L., et al. 2018, ApJ, 856, 23, doi: 10.3847/1538-4357/aaae09

Gaia Collaboration, Prusti, T., de Bruijne, J. H. J., et al. 2016, A&A, 595, A1, doi: 10.1051/0004-6361/201629272

Gaia Collaboration, Brown, A. G. A., Vallenari, A., et al. 2021, A&A, 649, A1, doi: 10.1051/0004-6361/202039657

Gray, D. F. 1992, The observation and analysis of stellar photospheres., Vol. 10 (Camb. Astrophys. Ser)

Green, G. M., Schlafly, E., Zucker, C., Speagle, J. S., & Finkbeiner, D. 2019, ApJ, 887, 93, doi: 10.3847/1538-4357/ab5362

Hattori, S., Foreman-Mackey, D., Hogg, D. W., et al. 2021, arXiv e-prints, arXiv:2106.15063. https://arxiv.org/abs/2106.15063

Henden, A. A., Templeton, M., Terrell, D., et al. 2016, VizieR Online Data Catalog, II/336

Hogg, D. W., Bovy, J., & Lang, D. 2010, arXiv e-prints, arXiv:1008.4686. https://arxiv.org/abs/1008.4686

Horne, J. H., & Baliunas, S. L. 1986, ApJ, 302, 757, doi: 10.1086/164037

Huang, C. X., Vanderburg, A., Pál, A., et al. 2020, Research Notes of the American Astronomical Society, 4, 204, doi: 10.3847/2515-5172/abca2e

Hunter, J. D. 2007, Computing in science & engineering, 9, 90

Husser, T.-O., Wende-von Berg, S., Dreizler, S., et al. 2013, A&A, 553, A6, doi: 10.1051/0004-6361/201219058

Johnson, J. A., Petigura, E. A., Fulton, B. J., et al. 2017, AJ, 154, 108, doi: 10.3847/1538-3881/aa80e7

Johnson, M. C., Dai, F., Justesen, A. B., et al. 2018, MNRAS, 481, 596, doi: 10.1093/mnras/sty2238

Jönsson, H., Holtzman, J. A., Allende Prieto, C., et al. 2020, AJ, 160, 120, doi: 10.3847/1538-3881/aba592

Katz, D., Sartoretti, P., Cropper, M., et al. 2019, A&A, 622, A205, doi: 10.1051/0004-6361/201833273

Kerr, R., Rizzuto, A. C., Kraus, A. L., & Offner, S. S. R. 2021, arXiv e-prints, arXiv:2105.09338. https://arxiv.org/abs/2105.09338

Kiman, R., Faherty, J. K., Cruz, K. L., et al. 2021, arXiv e-prints, arXiv:2104.01232. https://arxiv.org/abs/2104.01232

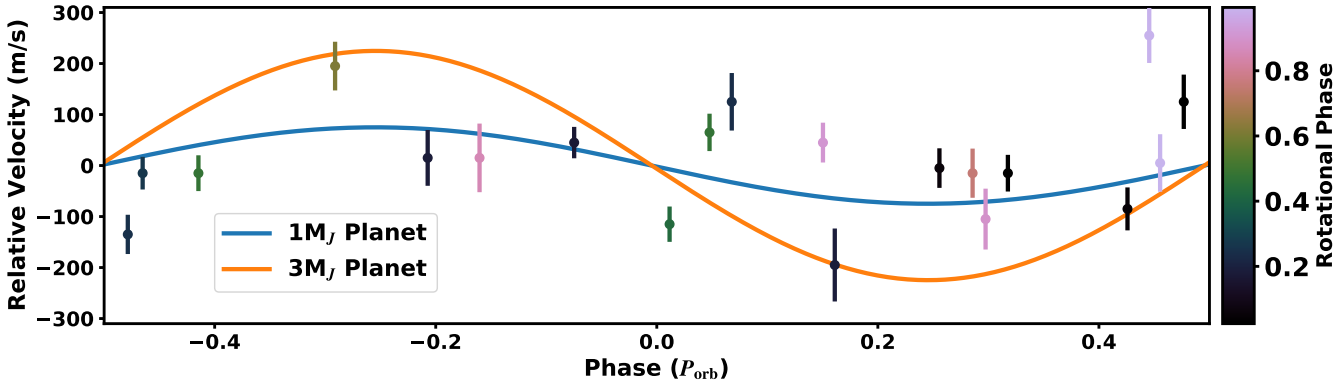

Figure 13. Radial velocities from APOGEE (Jönsson et al. 2020) for KOI-3876 as a function of the planet's orbital phase and colored by the rotational phase. The velocities rule out any companion more massive than $\simeq 2M_J$, ruling out any possibility of an eclipsing binary at the transit period. The scatter is larger than expected for the uncertainties by $\simeq$100m s^{-1}, but this is most likely due to stellar jitter common in young stars (Brems et al. 2019; Tran et al. 2021), and this is still far below the expected variation for a tight eclipsing binary.

Kipping, D. M. 2013, MNRAS, 435, 2152, doi: 10.1093/mnras/stt1435

Kounkel, M., & Covey, K. 2019, AJ, 158, 122, doi: 10.3847/1538-3881/ab339a

Kraus, A. L., Ireland, M. J., Huber, D., Mann, A. W., & Dupuy, T. J. 2016, AJ, 152, 8, doi: 10.3847/0004-6256/152/1/8

Kreidberg, L. 2015, PASP, 127, 1161, doi: 10.1086/683602

Krumholz, M. R., McKee, C. F., & Bland-Hawthorn, J. 2019, ARA&A, 57, 227, doi: 10.1146/annurev-astro-091918-104430

Lim, P. L. 2020, synphot, 1.0.1, Zenodo, doi: 10.5281/zenodo.3971036

Luo, A. L., Zhao, Y. H., Zhao, G., & et al. 2019, VizieR Online Data Catalog, V/164

Luo, A. L., Zhao, Y.-H., Zhao, G., et al. 2015, Research in Astronomy and Astrophysics, 15, 1095, doi: 10.1088/1674-4527/15/8/002

Mann, A. W., Newton, E. R., Rizzuto, A. C., et al. 2016a, AJ, 152, 61, doi: 10.3847/0004-6256/152/3/61

Mann, A. W., Gaidos, E., Mace, G. N., et al. 2016b, ApJ, 818, 46, doi: 10.3847/0004-637X/818/1/46

Mann, A. W., Dupuy, T., Kraus, A. L., et al. 2019, ApJ, 871, 63, doi: 10.3847/1538-4357/aaf3bc

Mann, A. W., Wood, M. L., Schmidt, S. P., et al. 2021, arXiv e-prints, arXiv:2110.09531. https://arxiv.org/abs/2110.09531

Masuda, K., & Winn, J. N. 2020, AJ, 159, 81, doi: 10.3847/1538-3881/ab65be

McQuillan, A., Aigrain, S., & Mazeh, T. 2013, MNRAS, 432, 1203, doi: 10.1093/mnras/stt536

McQuillan, A., Mazeh, T., & Aigrain, S. 2014, ApJS, 211, 24, doi: 10.1088/0067-0049/211/2/24

Meibom, S., Barnes, S. A., Latham, D. W., et al. 2011, ApJL, 733, L9, doi: 10.1088/2041-8205/733/1/L9

Meibom, S., Torres, G., Fressin, F., et al. 2013, Nature, 499, 55, doi: 10.1038/nature12279

Meingast, S., Alves, J., & Fürnkranz, V. 2019, A&A, 622, L13, doi: 10.1051/0004-6361/201834950

Miglio, A., Brogaard, K., Stello, D., et al. 2012, MNRAS, 419, 2077, doi: 10.1111/j.1365-2966.2011.19859.x

Morton, T. D. 2015a, isochrones: Stellar model grid package. http://ascl.net/1503.010

—. 2015b, VESPA: False positive probabilities calculator, Astrophysics Source Code Library. http://ascl.net/1503.011

Morton, T. D., Bryson, S. T., Coughlin, J. L., et al. 2016, ApJ, 822, 86, doi: 10.3847/0004-637X/822/2/86

Morton, T. D., & Winn, J. N. 2014, ApJ, 796, 47, doi: 10.1088/0004-637X/796/1/47

Nielsen, M. B., Gizon, L., Schunker, H., & Karoff, C. 2013, A&A, 557, L10, doi: 10.1051/0004-6361/201321912

Parviainen, H., & Aigrain, S. 2015, MNRAS, 453, 3821, doi: 10.1093/mnras/stv1857

Petigura, E. A. in prep, AJ

Petigura, E. A., Howard, A. W., Marcy, G. W., et al. 2017, AJ, 154, 107, doi: 10.3847/1538-3881/aa80de

Rampalli, R., Agüeros, M. A., Curtis, J. L., et al. 2021, arXiv e-prints, arXiv:2106.13250. https://arxiv.org/abs/2106.13250

Rebull, L. M., Stauffer, J. R., Bouvier, J., et al. 2016, AJ, 152, 113, doi: 10.3847/0004-6256/152/5/113

Rizzuto, A. C., Mann, A. W., Vanderburg, A., Kraus, A. L., & Covey, K. R. 2017, AJ, 154, 224, doi: 10.3847/1538-3881/aa9070

Santos, A. R. G., Breton, S. N., Mathur, S., & García, R. A. 2021, ApJS, 255, 17, doi: 10.3847/1538-4365/ac033f

Santos, A. R. G., García, R. A., Mathur, S., et al. 2019, ApJS, 244, 21, doi: 10.3847/1538-4365/ab3b56

Schlafly, E. F., & Finkbeiner, D. P. 2011, ApJ, 737, 103, doi: 10.1088/0004-637X/737/2/103

Skrutskie, M. F., Cutri, R. M., Stiening, R., et al. 2006, AJ, 131, 1163, doi: 10.1086/498708

Smith, J. C., Stumpe, M. C., Van Cleve, J. E., et al. 2012, PASP, 124, 1000, doi: 10.1086/667697

Stanford-Moore, S. A., Nielsen, E. L., De Rosa, R. J., Macintosh, B., & Czekala, I. 2020, ApJ, 898, 27, doi: 10.3847/1538-4357/ab9a35

Stassun, K. G., Oelkers, R. J., Pepper, J., et al. 2018, AJ, 156, 102, doi: 10.3847/1538-3881/aad050

Stassun, K. G., Oelkers, R. J., Paegert, M., et al. 2019, AJ, 158, 138, doi: 10.3847/1538-3881/ab3467

Stumpe, M. C., Smith, J. C., Van Cleve, J. E., et al. 2012, PASP, 124, 985, doi: 10.1086/667698

Tofflemire, B. M., Mathieu, R. D., & Johns-Krull, C. M. 2019, AJ, 158, 245, doi: 10.3847/1538-3881/ab4f7d

Tofflemire, B. M., Rizzuto, A. C., Newton, E. R., et al. 2021, AJ, 161, 171, doi: 10.3847/1538-3881/abdf53

Tran, Q. H., Bowler, B. P., Cochran, W. D., et al. 2021, AJ, 161, 173, doi: 10.3847/1538-3881/abe041

Tull, R. G., MacQueen, P. J., Sneden, C., & Lambert, D. L. 1995, PASP, 107, 251, doi: 10.1086/133548

Twicken, J. D., Jenkins, J. M., Seader, S. E., et al. 2016, AJ, 152, 158, doi: 10.3847/0004-6256/152/6/158

Van Cleve, J. E., Howell, S. B., Smith, J. C., et al. 2016, PASP, 128, 075002, doi: 10.1088/1538-3873/128/965/075002

van Saders, J. L., Ceillier, T., Metcalfe, T. S., et al. 2016, Nature, 529, 181, doi: 10.1038/nature16168

Walkowicz, L. M., & Basri, G. S. 2013, MNRAS, 436, 1883, doi: 10.1093/mnras/stt1700

Wood, M. L., Mann, A. W., & Kraus, A. L. 2021, arXiv e-prints, arXiv:2106.09040. https://arxiv.org/abs/2106.09040

Yee, S. W., Petigura, E. A., & von Braun, K. 2017, ApJ, 836, 77, doi: 10.3847/1538-4357/836/1/77

Ziegler, C., Tokovinin, A., Briceño, C., et al. 2020, AJ, 159, 19, doi: 10.3847/1538-3881/ab55e9

Table 5.

Gaia EDR3	α	δ	Gmag	$V_{\rm off}$	Spectral	TESS	Kepler	π	σ_π	$P_{\rm rot}$	$\sigma_{P_{\rm rot}}$	$P_{\rm rot}$	Li	$\sigma_{\rm li}$	RV	$\sigma_{\rm RV}$	RV
	(J2016)	(J2016)	(mag)	(km/s)	Class			(mas)	(mas)	(days)	(days)	ref	($m\AA$)	($m\AA$)	(km/s)	(km/s)	ref
2052827207364859264	290.44063	38.52357	12.605	0.000	G7.3	Y	Y	3.057	0.009	4.665	0.035	2, 3	134.0	18.0	-26.09	0.03	5
2101379205604338688	289.62522	40.70874	14.788	3.102	K5.3	N	Y	3.015	0.019	9.23	0.66	3	<40	...	-27.15	0.10	9
2052804323776522624	290.46921	38.20201	18.977	3.554	M3.9	N	N	3.036	0.172	...	...	...	...	...	...	...	...
2100939194794324608	289.80783	38.95042	10.829	0.478	F4.4	Y	N	3.024	0.012	...	...	...	<20	...	-27.03	0.18	5
2052954995531623040	291.28017	39.20070	14.355	4.348	K4.7	N	Y	3.055	0.016	13.849	0.035	1, 2, 3	...	...	...	...	...
2100967537279486336	290.14895	39.26079	18.451	3.806	M4.1	N	N	3.094	0.136	...	...	...	...	...	...	...	...
2051102868195719168	290.43983	37.73210	17.503	0.516	M3.2	N	N	3.019	0.069	...	...	...	...	...	...	...	...
2053037660761796096	290.86832	39.65124	17.902	0.605	M3.7	N	N	3.067	0.084	...	...	...	...	...	...	...	...
2052645379929910144	290.91118	38.33558	13.747	0.988	K2.8	N	Y	2.996	0.033	7.84	0.784	4	...	...	-27.05	3.02	6
2052559995978462208	291.61221	37.79730	11.75	3.744	F9.3	Y	Y	3.082	0.01	10.55	0.552	1, 3	...	...	-16.07	0.95	7
2100996639982248320	289.86923	39.64549	19.678	2.692	M3.7	N	N	3.083	0.322	...	...	...	...	...	...	...	...
2099426507311747200	289.44803	38.58778	17.385	0.897	M3.1	N	N	3.114	0.07	...	...	...	...	...	...	...	...
2052684790548985728	291.78531	38.46727	14.077	0.641	K4.6	N	N	3.009	0.038	...	...	...	...	...	...	...	...
2052858307226740352	290.54042	38.81248	11.42	0.350	F9.4	N	Y	2.978	0.019	4.419	0.347	2	<70	...	-25.11	0.16	5
2053046907832580992	291.12056	39.64699	16.939	0.389	M2.6	N	N	3.003	0.046	...	...	...	...	...	...	...	...
2099289446315734784	288.78892	37.90815	10.835	0.240	F4.3	Y	N	3.099	0.011	...	...	...	<20	...	-27.46	0.13	5
2053001690416510720	291.56724	39.60279	18.441	0.159	M4.5	N	N	3.104	0.122	...	...	...	...	...	...	...	...
2052887478644057472	289.93506	38.64045	14.636	0.506	K5.3	N	Y	3.145	0.018	1.529	0.017	1, 2, 3	...	...	-30.74	5.17	6
2052807794117101312	290.53790	38.25958	14.736	3.776	K5.4	N	Y	2.971	0.031	7.595	0.222	1, 2, 3	...	...	...	...	...
2052517145084325888	291.05028	37.29823	19.789	0.587	M4.1	N	N	3.002	0.33	...	...	...	...	...	...	...	...
2053028319213859072	290.64738	39.41039	20.044	2.510	M2.4	N	N	3.141	0.449	...	...	...	...	...	...	...	...
2053384286102387200	291.63783	39.87497	16.359	1.316	M2.7	N	N	3.008	0.037	...	...	...	...	...	...	...	...
2099371153774293888	288.14566	38.42085	13.864	0.791	K3.3	N	Y	3.018	0.025	7.556	0.049	1, 2, 3	...	...	-33.36	10.0	6
2053444896681432704	291.46297	40.21305	17.606	4.287	M3.8	N	N	3.093	0.076	...	...	...	...	...	...	...	...
2051172511083958400	289.48378	37.33728	20.024	1.298	M2.3	N	N	3.137	0.394	...	...	...	...	...	...	...	...
2053078450072688000	291.08713	40.21787	15.897	4.996	M0.3	Y	Y	3.112	0.03	26.792	0.394	1, 2, 3	...	...	...	...	...
2101290488760369920	288.83978	40.10791	16.391	4.143	M2.5	N	N	3.024	0.135	2.254	0.225	4	...	...	...	...	...
2101187134663932544	290.69156	40.59631	19.858	4.582	M3.3	N	N	3.084	0.312	...	...	...	...	...	...	...	...
2099510688671686656	288.69978	39.12272	18.18	2.451	M4.1	N	N	3.145	0.326	...	...	4	...	...	...	...	...

[a] Friends are targets less than 50 pc away and a tangential velocity within 5km s^{-1} of KOI-3876.

[b] Key for rotation period references: 1 = (McQuillan et al. 2013, 2014), 2 = (Nielsen et al. 2013), 3 = Santos et al. (2021, 2019), 4 = This work

[c] Indicates if the target had a light curve in *TESS* or *Kepler* of sufficient quality for running the Notch transit-search pipeline.

[d] Key for radial velocity references: 5 = Coude, 6 = LAMOSTDR5 (Luo et al. 2019), 7 = Gaia DR2 (Katz et al. 2019), 8 = APOGEE DR16 (Jönsson et al. 2020), 9 = CKS (Petigura in prep)